

Spin Ice

Michel J.P. Gingras

Department of Physics and Astronomy, University of Waterloo,
Waterloo, Ontario, N2L-3G1, Canada

and

Canadian Institute for Advanced Research/Quantum Materials Program
180 Dundas Street West, Suite 1400, Toronto, Ontario, M5G-1Z8, Canada
gingras@gandalf.uwaterloo.ca

Summary. Geometric frustration usually arises in systems that comprise magnetic moments (spins) which reside on the sites of a lattice made up of elementary triangular or tetrahedral units and which interact via antiferromagnetic nearest-neighbor exchange. Albeit much less common, geometric frustration can also arise in systems with strong non-collinear single-ion easy-axis (Ising-like) anisotropy and ferromagnetically coupled spins. This is what happens in some pyrochlore oxide materials where Ising-like magnetic rare earth moments (Ho^{3+} , Dy^{3+}) sit on a lattice of corner-shared tetrahedra and are coupled via effectively ferromagnetic (dipolar) interactions. These systems possess a macroscopic number of quasi-degenerate classical ground states and display an extensive low-temperature entropy closely related to the extensive proton disorder entropy in common water ice. For this reason, these magnetic systems are called spin ice. This chapter reviews the essential ingredients of spin ice phenomenology in magnetic pyrochlore oxides.

1.1 Introduction

In some geometrically frustrated magnetic systems, there exists an exponentially large number, Ω_0 , of degenerate classical ground states. This gives rise to an extensive residual, or zero point, ground state entropy, $S_0 = k_B \ln(\Omega_0)$. The most celebrated example of such a system is the triangular lattice with Ising spins interacting via nearest-neighbor antiferromagnetic exchange. Indeed, as shown by Wannier in 1950, this system remains disordered at all temperatures, with a ground state that has two spins up and one spin down (or vice versa) per triangle and has a zero point entropy per site $S_0 = 0.323 k_B$ [1]. However, the triangular Ising antiferromagnet was not the first condensed matter system identified as having a residual entropy. In fact, the first such system was not even a magnetic one. Fifteen years or so earlier, William Giauque (Chemistry Nobel Prize, 1949) and co-workers had performed thermodynamic measurements and determined that the solid phase of common water ice possesses an unaccounted residual entropy [2,3]. This result was soon explained by Linus Pauling (Chemistry Nobel Prize, 1954) in terms of a macroscopic number of proton (H^+) configurations in water ice arising from the mismatch between the

crystalline symmetry of ice and the local hydrogen bonding requirement of the water molecule [4].

Over the past ten years, a certain class of insulating magnetic materials in which the configurational disorder in the orientations of the magnetic moments is precisely the same as that of water ice have been the subject of numerous experimental and theoretical studies. Because of their analogy with water ice, these systems have been coined the name spin ice [5, 6, 7, 8, 9]. Most chapters in this book focus on geometrically frustrated antiferromagnets. The main reason for the interest in frustrated antiferromagnets is the pursuit of novel quantum ground states with exciting properties which, because of the increased quantum zero point motion caused by the frustration, lack conventional semi-classical long-range Néel order. This chapter differs in that the spin ices are frustrated Ising ferromagnets and where quantum fluctuations do not play a significant role. Yet, experimental and theoretical studies have revealed a great richness of equilibrium and non-equilibrium thermodynamic behaviors in spin ice systems [9]. This chapter reviews some of the salient elements of the spin ice phenomenology. It draws particular attention to the problem of water ice and the semi-formal origin of the Ising nature of the magnetic moments in spin ice materials, two topics that are not usually covered in detail in standard graduate solid state textbooks. It also reviews in some detail the mean-field theory of spin ices as this simple tool played a key role in uncovering the microscopic origin behind the emergence of the ice rules in real dipolar spin ice materials. We end the chapter with a brief discussion of research topics on spin ices that are of current interest.

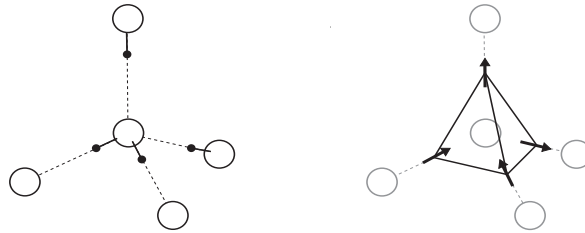


Fig. 1.1. Left: Local proton arrangement in water ice, showing O^{2-} ions (large white circles) and protons (hydrogen ions, H^+ , small black circles). Each O^{2-} is tetrahedrally coordinated with four other O^{2-} , with two near covalently bonded protons, and two further hydrogen bonded protons. In the hexagonal phase of ice, I_h , the low energy configurations obey the so-called Bernal-Fowler "ice rules" [10] where each O^{2-} oxide has "two-near" and "two-far" protons. Right: Same as left picture, but where the position of a proton is represented by a displacement vector (arrow) located at the midpoint of the $O^{2-} O^{2-}$ (oxide-oxide) bond. The "two-near/two-far" Bernal-Fowler ice rule then translates into a "two-in/two-out" configuration of the displacement vectors. The displacement vectors become the Ising magnetic moments in spin ice (see Fig. 1.2).

1.2 Water Ice, Pauling's Entropy and Anderson's Model

1.2.1 Water ice and Pauling's model

Water ice is a fascinating strongly correlated condensed matter system, not least because it exhibits a seemingly violation of the third law of thermodynamics. In the early 1930s, a series of remarkable specific heat experiments by William Giauque and co-workers found that the limiting low-temperature state of the common (hexagonal) state of water ice, referred to as I_h , is characterized by a residual entropy, $S_0 = 0.82 \pm 0.05 \text{ Cal/deg mol}$, that differs from zero by a value far in excess of experimental errors [2, 3]. In a famous 1935 paper, Linus Pauling showed that, because of its configurational proton disorder, I_h possesses a finite entropy at zero temperature estimated as 0.81 Cal/deg mol , hence very close to the experimental value.

The ice problem is a classic example of how the separation of energy scales in an interacting system can leave some effective low energy degrees of freedom inoperative and ultimately frustrated in a system's overall agenda in minimizing its energy at low temperature via local dynamical processes and over a finite, as opposed to infinite, amount of time. Here, the chemical binding energy of the water molecule is so strong, 221 kCal/mol , that its chemical structure is left essentially unaltered in the solid phase. Consequently, the ground state of water ice does not, or more precisely, dynamically cannot, minimize the electrostatic energy of a globally neutral ensemble of O^{2-} and H^+ ions. Rather, in the hexagonal ("wurtzite") and cubic ("sphalerite") phases of ice [11], the O^{2-} ions form an open tetrahedral structure, whose 109° angles accommodate almost perfectly that of the $H-O-H$ bonds of an isolated H_2O molecule. In the wurtzite phase, the bond length between two distinct O^{2-} ions is 2.76 \AA , while the covalent $O-H$ bond of a H_2O molecule is a much smaller 0.96 \AA . As the integrity of the molecular structure of H_2O is maintained in the solid phase, the minimum energy position of a H^+ proton is not at the midpoint between two O^{2-} ions. Instead, there are two equivalent positions for a proton lying on an $O-O$ bond. With the four-fold oxygen co-ordination in the hexagonal wurtzite structure, there is in effect one proton per $O-O$ bond on average. The constraint imposed by the energetically robust H_2O structure therefore results in the two so-called Bernal-Fowler ice rules which govern what are acceptable low-energy proton configurations in the hexagonal wurtzite structure [10]. The first ice rule states that there should only be one proton per $O-O$ on average. The second rule states that, in order for ice to consist of a hydrogen-bonded solid of water molecules, for each O^{2-} ions, two H^+ protons must be in a "near-to- O^{2-} " position, and two protons must be in a "far position" (see Fig. 1.1). From a solely electrostatic point of view, the protons would like to be as far apart as possible. The ice rules, implemented via the unaltered integrity of the H_2O water molecule, render the proton-proton interaction an effectively low-energy part of the problem, and frustrates it.

The ice rules were put forward by Bernal and Fowler in 1933 [10]. At that time, X-ray diffraction could only determine the lattice structure for the oxygen atoms. According to the first ice rule, Bernal and Fowler argued that the hydrogens must lie along the direct oxygen-oxygen line of contact (bond) between two H_2O molecules. They proposed a regular crystalline proton structure, presumably expecting that this would be the case. However, around the same time, Giauque and co-workers had already obtained compelling evidence for a residual zero point entropy in water

ice [2]. This led Pauling to his proposal, published in 1935, that the open tetrahedral structure of ice leads to many equivalent ways of satisfying the Bernal-Fowler ice rules, and hence to an extensive entropy [4].

Pauling put forward an elegant argument to estimate the configurational proton entropy. The argument goes as follows. First consider one mole of ice containing N_0 O^{2-} ions and, therefore, $2N_0$ $O-O$ bonds for the hexagonal structure of ice in which no two protons are on any given $O-O$ bond. That is, all bonds are taken to obey the first Bernal-Fowler ice rule. Each $O-O$ bond can be taken as having two possible positions for a proton. This gives $2^{(2N_0)}$ possible proton configurations for the whole system. Out of the 16 possible configurations associated with each oxygen, ten are energetically unfavourable: the OH_4^{2+} configuration, the 4 OH_3^+ configurations, the 4 OH^- configurations and the O^{2-} configuration. This leaves six configurations that satisfy the Bernal-Fowler rules as the allowed local proton configurations around each oxygen ion. An upper bound on the number of ground state configurations, Ω_0 , can therefore be estimated by reducing the above $2^{(2N_0)}$ configurations by a simple $6/16$ deviation weight factor for each oxygen ion. This gives $\Omega_0 = 2^{(2N_0)} (6/16)^{N_0} = (3/2)^{N_0}$. The corresponding configurational entropy, $S_0 = k_B \ln(\Omega_0) = N_0 k_B \ln(3/2) = 0.81 \text{ Cal/deg mol}$, is in excellent agreement with the residual entropy of $0.82 \pm 0.05 \text{ Cal/deg mol}$ determined by Giauque and Stout [5]. Pauling's calculation neglects the global constraint on the number of protons as well as the local constraints coming from closed loops on the wurtzite lattice. Nevertheless, Pauling's estimate has been shown to be accurate to 1–2% [12].

1.2.2 Cation ordering in inverse spinels and antiferromagnetic pyrochlore Ising model

In a 1956 paper [13], Anderson investigated the problems of cation ordering in the so-called inverse spinel materials and that of magnetic ordering in normal spinels. To a first approximation, both of these problems map onto the problem of an Ising model with antiferromagnetic nearest-neighbor exchange interaction on the B-site of the spinel lattice. This lattice is structurally identical to the pyrochlore lattice shown in Fig. 1.2. For a discussion of magnetic ordering in spinels, see the Chapter by Takagi in this book.

Consider first the problem of cation ordering in the inverse spinel. The associated minimum energy problem consists in placing $+$ and $-$ signs on the pyrochlore lattice (see Fig. 1.2) in a ratio 1:1 such that the number of $+-$ pairs is maximized. This condition is satisfied with two $+$ and two $-$ signs for each tetrahedron. The center of the tetrahedra in the spinel lattice are arranged with respect to each other on the same lattice as the oxygen ions in the cubic phase of water ice (I_c). As shown in Fig. 1.2, the spinel lattice and, equivalently, the pyrochlore lattice, consists of alternating "upward" and "downward" tetrahedra. Consequently, the problem of $+$ and $-$ charge organization problem maps onto an ice rule problem if a $+$ sign corresponds to a "proton near" on an upward tetrahedron and a "proton far" on a downward tetrahedron, and vice-versa for a $-$ sign. Neglecting the same constraints that Pauling neglected for the water ice problem, the problem of cation ordering in inverse spinels therefore maps onto an ice-like problem, and is therefore characterized by a Pauling zero point entropy [13]. The problem of cation ordering is also manifestly the same as that of an antiferromagnetic Ising model on the pyrochlore lattice, where $+$ represents a spin up and $-$ represents a spin down. It is

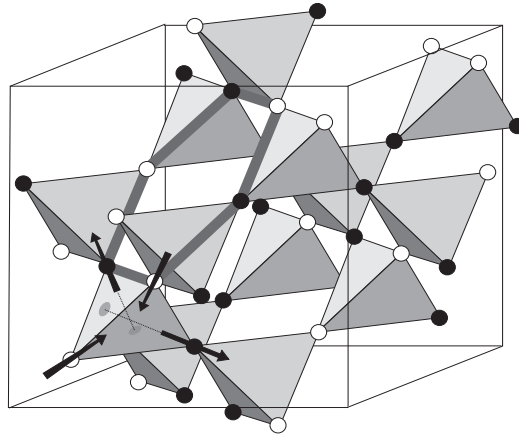


Fig. 1.2. Pyrochlore lattice of corner-sharing tetrahedra, as occupied by Ho^{3+} and Dy^{3+} in the $\text{Ho}_2\text{Ti}_2\text{O}_7$ and $\text{Dy}_2\text{Ti}_2\text{O}_7$ spin ice materials. The magnetic rare-earth Ising moments occupy the corners of the tetrahedra, as shown on the lower left "downward" tetrahedron of the lattice (arrows). The spins here are the equivalents of the proton displacement vectors in Fig. 1.1. Each spin axis is along its local $[111]$ quantization axis, which goes from one site to the middle of the opposing triangular face (as shown by the disks) and meets with the three other $[111]$ axes in the middle of the tetrahedron. In the spin ice materials, the "two-in/two-out" condition arises from the combined effect of magnetic (exchange and dipole-dipole) interactions and the strong Ising anisotropy. For clarity, other spins on the lattice are denoted by black and white circles, where white represents a spin pointing into a downward tetrahedron while black is the opposite. The entire lattice is shown in an ice-rules state (two black and two white sites for every tetrahedron). The hexagon (thick gray line) pertains to the loop excitations used in the "loop Monte Carlo" simulations discussed in Section 1.4.3. The shown hexagon is the smallest possible loop move involving multiple spins, and which corresponds to reversing all spins on the loop to produce a new ice-rules obeying state. The reversal of spins on closed loops are the lowest-energy excitations that allow the system to explore the quasi-degenerate ice rule manifold of dipolar spin ice at low temperatures. (Figure reprinted with permission from R. G. Melko et al., Phys. Rev. Lett. 87, 067203 (2001). Copyright 2001 by the American Physical Society.)

interesting to note that in the context of an antiferromagnetic Ising model on the pyrochlore lattice, Anderson's model was the second example of what would now be referred to as a frustrated antiferromagnet, the first one being the problem of the Ising antiferromagnet on the triangular lattice studied by Wannier in 1950 [1].

Anderson's model is an important paradigm for frustrated magnetic systems of interacting spins that reside on the sites of a lattice of corner-shared triangles or tetrahedra, as occurs in kagome, garnet and pyrochlore lattices. Yet, there are no known realizations of Anderson's Ising antiferromagnet on the pyrochlore lattice.

The reason is that the pyrochlore lattice has a cubic symmetry, and there is no energetic reason permitted by symmetry that would favor a unique global \hat{z} Ising direction to the detriment of another global direction. However, a system of antiferromagnetically coupled isotropic Heisenberg spins on the pyrochlore lattice is realistic. This problem was the topic of an important 1979 paper [14]. In that work, Villain anticipated the failure of the classical Heisenberg pyrochlore antiferromagnet to develop long range order down to zero temperature [15,16] and coined the name collective paramagnet to this system – a terminology that one may want to ascribe to the classical variant of the more modern terminology of spin liquid used in quantum spin systems. Because they lack the intrinsic propensity to develop classical long range magnetic order, antiferromagnetic materials with Heisenberg spins that reside on a pyrochlore lattice are expected to be excellent candidates to display exotic quantum mechanical ground states. It is the anticipation of the observation of interesting magnetic and thermodynamic behaviors in the broad family of magnetic pyrochlore oxide materials, of generic formula $A_2B_2O_7$, that led at the end of the 1980's to the rapid rise of experimental and theoretical efforts devoted to the study of these systems [17,18]. It is also this general scientific endeavour that led to the discovery of spin ice [5,6,7], a novel class of frustrated ferromagnetic Ising systems, close analogues of both water ice and the cation ordering in spinels. This discovery also led to the rebirth of a disguised variant of Anderson's antiferromagnetic Ising model [13] on the pyrochlore lattice.

1.3 Discovery of Spin Ice

1.3.1 Rare earth pyrochlore oxides – generalities

Before reviewing the discovery of spin ice materials and the spin ice problematics, we first briefly discuss some general aspects of the pyrochlore oxides, the broader class of materials to which spin ices belong. We also review the elementary background behind the origin of the magnetism in the rare earth ions involved in spin ices, how they acquire their strong Ising nature, and what the predominant interactions between the magnetic ions are.

The $A_2B_2O_7$ magnetic pyrochlore oxides form a broad family of materials that exhibit a wide range of interesting thermodynamic and magnetic phenomena, a number of which are still poorly understood [17,18]. Here, both the trivalent A^{3+} ion (A is a rare earth element such as Gd, Tb, Dy, Ho, etc, or Y) and the tetravalent B^{4+} ion ($B = Ti, Sn, Mo, Mn$) reside on two independent and interpenetrating pyrochlore sublattices. Figure 1.2 shows only one of those two sublattices, say the A sublattice. In $A_2B_2O_7$, one can have either the A or the B sublattice occupied by a magnetic ion, as in $Tb_2Ti_2O_7$ [19] and $Y_2Mo_2O_7$ [20], respectively, or both sites can be occupied by a magnetic ion such as in $Tb_2Mo_2O_7$ [21]. As discussed by Villain already thirty years ago [14], the pyrochlore lattice is highly frustrated when the ions carry an isotropic Heisenberg spin and interacts with nearest neighbors via an antiferromagnetic exchange coupling. The pyrochlore oxides can be metallic (e.g. $Nd_2Mo_2O_7$, which displays an interesting anomalous Hall effect [22]) or they can be insulating, as is the case for the $A_2Ti_2O_7$ and $A_2Sn_2O_7$ series [17,18]. In this chapter, we shall restrict ourselves to the insulating $A_2Ti_2O_7$ and $A_2Sn_2O_7$ series with Dy and Ho as magnetic ion; Ti^{4+} and Sn^{4+} are non-magnetic. That is, we are

dealing with only one magnetic pyrochlore sublattice, the A sublattice, in $A_2B_2O_7$, which we henceforth simply refer to "the pyrochlore lattice". Neglecting spin-spin interactions [23], the Tb^{3+} ion in $Tb_2Ti_2O_7$ and $Tb_2Sn_2O_7$ would also be described as an Ising spin at sufficiently low temperatures [24,25]. However, interactions make the strictly Ising model description of these two materials invalid [23].

The pyrochlore lattice can be conveniently described as a face-centered cubic (FCC) lattice with a primitive ("upward", or "downward") tetrahedron basis cell of four sites (see Fig. 1.2). The pyrochlore lattice possesses a trigonal (threefold rotational) symmetry with respect to any of the four equivalent $\langle 111 \rangle$ cubic lattice directions (i.e. the diagonals of the cubic cell in Fig. 1.2). For each of the four sites in the tetrahedron unit cell, it will prove convenient to use as local \hat{z}_i axis of spin quantization the specific $\langle 111 \rangle$ cube diagonal that passes through a given site i and the middle of the opposite triangular face (see Fig. 1.2).

One should note that common water ice at atmospheric pressure, ice I_h , has a hexagonal structure while the magnetic pyrochlore lattice has a cubic symmetry. Strictly speaking, the Ising pyrochlore problem is equivalent to cubic ice, I_c , and not the hexagonal I_h phase. However, this does not modify the "ice-rule" analogy (or mapping) or the close connection between the orientation of the magnetic moments in spin ice and the local proton coordination in water ice.

1.3.2 Microscopic Hamiltonian towards an effective Ising model

The spin-orbit interaction is large in rare-earth ions and the total angular momentum, $J = L + S$, can be taken as a good quantum number. For a given ion, one can apply Hund's rules to determine the isolated (vacuum) electronic ground state. For example, Tb has an electronic configuration $[Xe]4f^9 6s^2$ and Tb^{3+} has $[Xe]4f^8$ as electronic ground state configuration. Following Hund's rules, one finds that $L=3$ and $S=3$, hence $J=6$ for Tb^{3+} and the spectroscopic notation for the ground multiplet is 7F_6 . Similarly, one finds $J=8$ for $Ho_2Ti_2O_7$ and $J=15/2$ for $Dy_2Ti_2O_7$. Electrostatic and covalent bonding effects, which originate from the crystalline environment, lead to a lifting of the otherwise free ion ground state $(2J+1)$ -fold electronic degeneracy. This is the so-called crystal field effect. The theoretical description of crystal field effects going beyond the simple Coulomb point charge description of the charges surrounding a rare earth ion, and which includes covalency effects and admixing between electronic multiplets, is a rather technical problem which we shall not discuss here. In the forthcoming discussion, we will merely assume that the single-ion crystal field energy levels (of the non-interacting ions) have been "suitably" determined. This can be done, for example, via experimental spectroscopic methods (e.g. optical spectroscopy, inelastic neutron scattering, etc). Such a spectroscopic approach allows to determine the transition frequencies between crystal field levels and their intensities which can then be described by a so-called crystal field Hamiltonian, H_{cf} (see for example Refs. [24,25,26]). We shall return to this point shortly. Ideally, one would like to make sure that the energy levels so-determined are not strongly "dressed" (i.e. affected, or renormalized) by inter-ion interactions described by H_{int} . This can sometimes be done by considering a highly magnetically diluted variant of the system of interest [25]. This leads us to introduce the Hamiltonian, H , needed to describe the minimal physics at stake:

$$H = H_{cf} + H_Z + H_{int} : \quad (1.1)$$

Here H_{cf} is the crystal-field Hamiltonian responsible for the lifting of the degeneracy of the otherwise free single-ion electronic ground state. Its energy eigenstates are the above crystal-field energy levels. As a first approximation, one can express H_{cf} in terms of polynomial functions of the $J_{i,z}$ and $J_{i,\pm} = J_{i,x} \pm iJ_{i,y}$ components of the angular momentum operator J . For the local symmetry of the rare-earth ions at the A site in $A_2B_2O_7$, one writes H_{cf} [24,25,26] as

$$H_{cf} = \sum_i \sum_{l,m} B_l^m O_l^m(J_i); \quad (1.2)$$

where B_l^m are the crystal-field coefficients and $O_l^m(J_i)$ are the equivalent crystal-field operators. Spectroscopic measurements allow to determine the B_l^m via a fitting procedure of the energy levels with further constraints from the observed transition intensities [24,26]. Because of the Wigner-Eckart theorem, $l \leq 6$ for $L=3/4$ elements. For example, $O_2^0 = 3J_z^2 - J(J+1)$, $O_4^0 = 35J_z^4 - (30J(J+1) - 25)J^2 + 3J^2(J+1) - 6J(J+1)$ and $O_4^{-3} = c[J_z; J_{\pm}^3 - J_{\mp}^3]_{\pm}$ with $[A; B]_{\pm} = (AB + BA)_{\pm} = 2, c_{\pm} = 1/2$ and $c = \sqrt{2}$ (see Refs. [27,28,29]).

In Eq. 1.1 $H_Z = g_B \mu_B \sum_i J_i$ is the Zeeman energy describing the interactions of the rare earth magnetic ions with the magnetic field B ; g_L is the Lande factor and μ_B is the Bohr magneton. Finally, H_{int} describes the interactions between the ions. We consider the following form for H_{int} :

$$H_{int} = \frac{1}{2} \sum_{(ij)} J_{ij} J_i \cdot J_j + \frac{0}{4} \sum_{(ij)} \frac{(g_L \mu_B)^2}{2r_{nn}^3} \frac{(J_i \cdot J_j - 3J_i J_j \cdot J_j)}{(r_{ij} = r_{nn})^3}; \quad (1.3)$$

where $r_{ij} = r_{ij} \hat{r}_{ij}$ with r_i the position of ion i . Here J_{ij} is the microscopic quantum mechanical exchange constant between ions i and j . We use the convention that $J_{ij} < 0$ is antiferromagnetic and $J_{ij} > 0$ is ferromagnetic. Note that in Eq. (1.3), the two sums are carried over all ions i and j , hence there is double-counting, and this is why there is a pre-factor $1/2$ in front of each sum. The first term "originates" from the interactions between the "real" electronic spins, S_i and S_j . For simplicity, we only consider here an effective isotropic "exchange" between the total angular momenta J_i and J_j with exchange interactions J_{ij} . Such description has proven adequate to describe the physics of spin ice materials [30,31,32,33]. The four distinct types of symmetry-allowed anisotropic exchange interactions on the pyrochlore lattice are described in Refs. [34,35]. The second term is the long range magnetostatic dipole-dipole interaction with r_{nn} the distance between nearest neighbors. The pyrochlore oxides have a conventional cubic unit cell of size $a = 10\text{\AA}$ with 16 ions (i.e. 4 "upward" or "downward" primitive tetrahedron basis cells, see Fig. 1.2) per conventional cubic unit cell and $r_{nn} = (a/\sqrt{2}) = 7.07\text{\AA}$. We now discuss the relative energy scales set by H_{cf} , H_Z and H_{int} .

By far, for the $(Ho,Dy)_2(Ti,Sn)_2O_7$ materials, which we will show later are spin ices, H_{cf} sets the largest energy scale in the problem. In these four materials, the spectrum of H_{cf} consists of a ground state doublet separated by an energy gap, Δ , of typically 300 K , to the first excited state. The Lande factor g_L of Ho^{3+} and Dy^{3+} is $5/4$ and $4/3$, respectively, and $\mu_B = 9.27 \times 10^{-24} \text{ J/T} = 0.671 \text{ K/T}$ in H_Z . In other words, even for a field of 20 T , which is about the largest field accessible via commercial in-house magnets, the Zeeman energy scale is of the order of 10 K , hence much smaller than Δ . Consequently, when calculating the properties of

$(\text{HoDy})_2(\text{TiSn})_2\text{O}_7$ at temperatures $T < 10$ K and in magnetic fields less than 20 T or so, one can safely consider only the magnetic crystal-field ground state doublet of Ho^{3+} and Dy^{3+} and ignore the susceptibility contributions from the excited states as well as the van Vleck susceptibility. The interaction part, H_{int} , deserves particular attention. In insulating magnetic rare earth materials, the unfilled 4f spin-carrying orbitals of the rare earth ion are shielded by 5s and 5p orbitals and the 4f orbital overlap between the rare earth ions and between rare earths and O^{2-} is therefore small. Consequently, the effective J_{ij} exchange coupling between rare earth ions is much smaller in insulating rare earth oxides compared to that of transition metal oxides. For example, a typical value for J_{ij} for nearest neighbors, J , is $J = 66$ mK in DyTiO_3 [30,33]. We can also estimate the dipolar energy scale, $D = \frac{1}{4}(\frac{g_L}{r_{\text{nn}}})^2 = (4 \frac{r_{\text{nn}}}{r_{\text{nn}}})^2$. Plugging in a value $r_{\text{nn}} = 3.5$ Å and $g_L = 4/3$, we get $D = 25$ mK [30,33]. Comparing J and D with $T = 300$ K, one sees that the interaction part H_{int} of the full Hamiltonian H is very small compared to the crystal-field part, H_{cf} [36]. In practice, this means that the independent/non-interacting single-ion crystal-field eigenstates of H_{cf} form a very convenient basis to describe the Hilbert space of interacting Dy^{3+} and Ho^{3+} ions in $(\text{HoDy})_2(\text{TiSn})_2\text{O}_7$. In particular, since the scale of H_{int} is so small compared to H_{cf} , one can, for all practical purposes, neglect all the excited states of H_{cf} and work with a reduced Hilbert space solely spanned by the two degenerate states of the ground doublet for each magnetic sites. In such a problem, where the high-energy sector of the theory is so well separated from the low-energy sector, it is convenient to introduce a so-called effective Hamiltonian, H_{e} , that operates only within the low-energy sector. The Chapter by Mila and Schmidt in this book describes the general methodology as to how to derive a H_{e} for a given interacting system where there are well separated "reference" energy sectors. For the spin ices, the lowest order of the perturbation theory which defines H_{e} is amply sufficient; i.e.

$$H_{\text{e}} = PH_{\text{int}}P \quad (1.4)$$

with P , the projector in the low-energy sector, defined as

$$P = \sum_{fkg} |j_{0,fkg}\rangle \langle j_{0,fkg}| \quad (1.5)$$

where

$$|j_{0,fkg}\rangle = \sum_{i=1}^N |j_{i,0}^{(k_i)}\rangle \quad (1.6)$$

Here $|j_{i,0}^{(k_i)}\rangle$ is the k_i^{th} state of the single-ion crystal-field ground doublet of rare earth ion i . Since H_{int} is a pairwise Hamiltonian, H_{e} is, to lowest order and given by Eq. (1.4), also a pairwise effective Hamiltonian. One can then determine H_{e} by considering two ions each in one of the two states, $|j_{i,0}^{(k_i=+)}\rangle$ and $|j_{i,0}^{(k_i=-)}\rangle$, of their respective crystal-field ground doublet. Hence, the effective Hamiltonian H_{e} is a 4×4 matrix. At this point, we need to return to the crystal-field problem and discuss the nature of the non-interacting $|j_{i,0}^{(k_i=)}\rangle$ states that make each of the single-ion ground doublet.

From inelastic neutron measurements, it is found that $|j_{i,0}^{(k_i=+)}\rangle$ and $|j_{i,0}^{(k_i=-)}\rangle$ for Ho_2TiO_7 are $|j_{i,0}^{(k_i=)}\rangle$ with $J = 8$ mJ and $J = -8$ mJ, with negligible contributions from

other $jJ = 8; m_J$ components. By rescaling the crystal field parameters determined for $\text{Ho}_2\text{Tl}_2\text{O}_7$ one can determine the crystal field parameters for $\text{Dy}_2\text{Tl}_2\text{O}_7$ [24]. One finds for the latter material $j_{i;0}^{(k_i=)} i$ $jJ = 15=2; m_J = 15=2i$ with again negligible weight from other $jJ = 15=2; m_J$ components [24]. It is important to recall the above discussion about the choice of the \hat{z}_i quantization direction. Here, the magnetic quantum number m_J eigenstate of J_z refers to the component of J_i along the local \hat{z}_i direction that points along one of the four cubic h111i directions. Calculating the matrix elements of $P H_{\text{int}} P$, one finds that, for both $\text{Ho}_2\text{Tl}_2\text{O}_7$ and $\text{Dy}_2\text{Tl}_2\text{O}_7$, the only significant matrix elements are $h_{i;0}^{(k_i=)} j_{i;0}^{(k_i=)} i$ J . The physical meaning is simple. In both $\text{Ho}_2\text{Tl}_2\text{O}_7$ and $\text{Dy}_2\text{Tl}_2\text{O}_7$, the magnetic moment can, for all practical purposes, only point parallel or antiparallel to the local [111] direction; we are dealing with a local h111i Ising model!

It is useful to write down the set of local \hat{z}_i quantization axis (i.e. \hat{z}_i k h111i axis). We take $\hat{z}_1 = \frac{1}{\sqrt{3}}(\hat{x} + \hat{y} + \hat{z})$, $\hat{z}_2 = \frac{1}{\sqrt{3}}(\hat{x} - \hat{y} + \hat{z})$, $\hat{z}_3 = \frac{1}{\sqrt{3}}(\hat{x} + \hat{y} - \hat{z})$ and $\hat{z}_4 = \frac{1}{\sqrt{3}}(\hat{x} - \hat{y} - \hat{z})$, with $\hat{z} \cdot \hat{z} = 1=3$ for ϵ . To proceed formally, one could re-express the above 4 4×4 matrix representing H_e in terms of tensor products of Pauli matrices, $\sigma_i^i \sigma_j^j$ where we are here using a local orthogonal $\{x_i; y_i; z_i\}$ frame [23], where $\sigma_i = x_i; y_i; z_i$. Had we kept the full $jJ; m_J$ decomposition of $j_{i;0}^{(k_i=)} i$, one would have found that the coefficient of the $\sigma_i^{z_i} \sigma_j^{z_j}$ term has by far the largest coefficient in H_e . We thus end up with a classical model with Ising spins pointing parallel or antiparallel to their local [111] direction.

Alternatively, one could have proceeded much more straightforwardly and simply replace

$$J_i \rightarrow jJ_z i j \frac{z_i}{\sqrt{3}} \hat{z}_i \quad (1.7)$$

right at the outset, and use $jJ_z i j = 8$ for $\text{Ho}_2\text{Tl}_2\text{O}_7$ and $jJ_z i j = 15=2$ for $\text{Dy}_2\text{Tl}_2\text{O}_7$. Indeed, this is what was implicitly done in most previous numerical studies of dipolar spin ice [7, 30, 31, 32, 37, 38]. Since there are no other components σ_i^i with $i \in \{z_i\}$ that do not commute among themselves left in H_e , we have a strictly classical Ising model for H_e . One can therefore work in the basis of eigenstates of $\sigma_i^{z_i}$ and, henceforth, we merely treat $\sigma_i^{z_i} = \pm 1$ as a classical variable. Admittedly, the discussion here leading to H_e as a classical Ising model for the Dy-based and Ho-based oxyde pyrochlores is rather academic. However, as mentioned earlier in Section 1.3.1 it is not so for $\text{Tb}_2\text{Tl}_2\text{O}_7$ [19] and $\text{Tb}_2\text{Sn}_2\text{O}_7$ [39]. Indeed, for these two materials, the energy gap separating the ground doublet and the excited doublet is not so large compared to the exchange and dipole-dipole interactions. In that case, higher order terms in the perturbation expansion leading to H_e must be retained (again, see the chapter by Mila and Schmilt) in order to derive a proper quantum theory of this material, as was recently done for a simple model of $\text{Tb}_2\text{Tl}_2\text{O}_7$ [23].

Returning to H_{int} above, and writing $J_i \rightarrow jJ_z i j \frac{z_i}{\sqrt{3}} \hat{z}_i$, we arrive at our effective classical h111i pyrochlore Ising model

$$H_{\text{DSM}} = \frac{1}{2} \sum_{(i,j)} J_{ij} (\hat{z}_i - \hat{z}_j) \frac{z_i}{\sqrt{3}} \frac{z_j}{\sqrt{3}} + \frac{D}{2} \sum_{(i,j)} \frac{(\hat{z}_i - \hat{z}_j) \cdot \hat{r}_{ij}}{(r_{ij} = r_{\text{nn}})^3} \frac{z_i}{\sqrt{3}} \frac{z_j}{\sqrt{3}}; \quad (1.8)$$

which we shall henceforth refer to as the "dipolar spin ice model" (DSM). Here we have written $J_{ij} = J_{ij} hJ_z i^2$ and $D = \mu_0 (g_L \mu_B hJ_z i)^2 = (4 \pi r_{\text{nn}}^3)$. Note that the variables $\sigma_i^{z_i} = \pm 1$ have become simple labels indicating whether the z_i -component of J_i points "in" or "out" of a primitive tetrahedron unit cell characterized by the

above set $\hat{z}_1; \hat{z}_2; \hat{z}_3; \hat{z}_4$ (see Fig. 1.2). Having established that the magnetic Dy^{3+} and Ho^{3+} ions in $\text{Dy}_2\text{T}_{1-x}\text{O}_7$ and $\text{Ho}_2\text{T}_{1-x}\text{O}_7$ should be described by effective classical Ising spins at temperatures much lower than the lowest crystal field gap, we can now proceed to discuss the experimental behavior of these two materials, and how the spin ice phenomenology arises.

1.3.3 Discovery of spin ice in $\text{Ho}_2\text{T}_{1-x}\text{O}_7$

In a 1997 paper, Harris, Bramwell and collaborators reported the results of a neutron scattering study of $\text{Ho}_2\text{T}_{1-x}\text{O}_7$ [5]. They found that, in zero applied magnetic field, no evidence of a transition to long range order could be detected down to 0.35 K via neutron scattering, while muon spin relaxation results could rule out a transition down to 0.05 K [6]. The most surprising part of those results was that the Curie-Weiss temperature, T_{CW} , was found to be positive with $T_{CW} = +1.9$ K, hence indicating overall ferromagnetic interactions. Naively, one would have expected such a three-dimensional cubic system with ferromagnetic interactions to develop long range order at a critical temperature of the same order of magnitude as T_{CW} . It was also found that the magnetic field dependence of the neutron scattering intensity depends on the protocol followed to magnetize the sample [40]. In other words, the system displayed a history dependence reminiscent of what is observed in random spin glasses [41], although no significant random disorder is present in $\text{Ho}_2\text{T}_{1-x}\text{O}_7$.

The authors of Refs. [5,6] proposed that the strong local [111] Ising anisotropy of Ho^{3+} in $\text{Ho}_2\text{T}_{1-x}\text{O}_7$ frustrates the development of ferromagnetic order. They considered a simple model of ferromagnetically coupled h111i Ising spins on the pyrochlore lattice [42]. By doing so, they established the connection between their model and that of Pauling's model for the problem of proton disorder in water ice, hence coining the name spin ice model to their model (see Fig. 1.1). For clarity sake, and since we shall discuss below the important role that long range dipole-dipole interactions play in spin ice materials, we relabel Harris et al.'s model as nearest-neighbor spin ice model, in order to distinguish it from the dipolar spin ice model (DSM) of Eq. (1.8). We discuss in the next section this nearest-neighbor spin ice model and show that it has the same residual entropy as water ice.

1.3.4 Nearest-neighbor ferromagnetic h111i Ising model and Pauling's entropy

Nearest-neighbor spin ice model

Consider a simplified version of the Ising Hamiltonian in Eq. (1.8) where the dipolar interaction coefficient is set to $D = 0$ for the time being and where we restrict the exchange interactions, J_{ij} , solely to nearest neighbors. We thus have

$$H_{nn} = \sum_{\langle ij \rangle} J (\hat{z}_i \cdot \hat{z}_j) \quad (1.9)$$

with the convention that the nearest-neighbor exchange $J > 0$ is ferromagnetic while $J < 0$ is antiferromagnetic. Taking $\hat{z}_i \cdot \hat{z}_j = 1/3$ for nearest neighbors on the pyrochlore, we have:

$$\begin{aligned}
H_{nn} &= \sum_{\langle ij \rangle} J_{ij} z_i z_j \\
&= \sum_{\langle ij \rangle} J \left(\frac{1}{3} \right) \sum_{\langle ij \rangle} z_i z_j \\
&= \frac{J}{3} \sum_{\langle ij \rangle} z_i z_j :
\end{aligned} \tag{1.10}$$

We can rewrite Eq. (1.10) as [16]

$$H_{nn} = \frac{J}{6} (L)^2 \frac{2N}{3} J \tag{1.11}$$

where the $\sum_{\langle ij \rangle}$ is now carried over each "upward" and "downward" tetrahedron units labelled by i , with a total of N "upward" and "downward" tetrahedra, and where L is the total spin on unit i , defined as

$$L = z_1 + z_2 + z_3 + z_4 : \tag{1.12}$$

From Eq. (1.10), one can appreciate the "first magic" of spin ice. We will discuss the "second magic" of spin ice in Section 1.4.1. By starting with a ferromagnetic nearest-neighbor exchange, $J > 0$ in Eq. (1.9), one ends up with z_i Ising variables that are now coupled via an effective antiferromagnetic coupling constant in Eq. (1.10). This is the same model as Anderson's frustrated antiferromagnetic pyrochlore Ising model used to describe the problem of cation ordering in inverse spinels [13]. The ferromagnetic hllli pyrochlore Ising model is therefore frustrated and, just as Anderson's model, it must possess a residual Pauling entropy.

In terms of H_{nn} in Eq. 1.11, the ground state configuration on a single tetrahedron for antiferromagnetic $J < 0$ consists of all $z_i = +1$ or all $z_i = -1$. In terms of the "real" J_i spins in Eq. 1.3, this corresponds to all J_i pointing "in" or all J_i pointing "out" of a reference tetrahedron unit cell. Globally, there are only two such states and, upon cooling the system, a second order transition to a four sublattice antiferromagnetic Neel ordered state in the three-dimension Ising universality class occurs. The four sublattice Neel ordered phase described in terms of the J_i maps onto a ferromagnetic ground state in terms of the z_i . The pyrochlore lattice with antiferromagnetically coupled hllli spins is therefore not frustrated. Conversely, for ferromagnetic $J > 0$, the z_i Ising variables are effectively coupled antiferromagnetically and the ground state on a single tetrahedron is 6-fold degenerate, arising from the condition $z_1 + z_2 + z_3 + z_4 = 0$ on each tetrahedron, from Eq. (1.12), i.e., two positive and two negative z_i . This is the incipient spin configuration leading to the extensive Pauling entropy of spin ice in the thermodynamic limit [7].

We now discuss how the nearest-neighbor spin ice model possesses a Pauling entropy. We invite the reader to refer to Fig. 1.1 where a more direct physical, or geometrical, connection between the z_i configurations in the spin ice problem and that of the "real" proton positions in water ice is illustrated.

Pauling entropy of the nearest-neighbor spin ice model

The macroscopically degenerate ground states that are often characteristic of frustrated systems can be understood in terms of an underconstraint argument [16].

That is, the extensive degeneracy arises from the difference between the number of constraints necessary to determine a ground state and the number of degrees of freedom that the system possesses. By following Pauling's heuristic argument for water ice, one can calculate the residual entropy of spin ice. Consider Anderson's Ising pyrochlore antiferromagnet, to which the local hilli pyrochlore Ising model maps, as discussed in Section 1.2.2. The ground state condition is "under-constrained", demanding only that the total magnetization, L , of the four Ising spins on each tetrahedron fulfills $L = 0$. Six of the $2^4 = 16$ possible spin configurations satisfy this condition. Counting 2^4 configurations for each tetrahedron gives, for a system of N spins and $N=2$ "upward" and "downward" tetrahedra, $(2^4)^{N/2} = 4^N$ microstates. This number drastically overestimates the exact total of 2^N microstates for N Ising spins. The reason is that each spin is shared between two tetrahedra, hence the above 16 configurations on each tetrahedron are not independent. Borrowing Pauling's argument, we allocate 2^2 states per tetrahedron and, assuming that 6=16 of them satisfy the constraint, we obtain a ground state degeneracy $\Omega_0 = (6/16)^{N/2} = (3/2)^{N/2}$. The corresponding entropy, $S_0 = k_B \ln(\Omega_0) = (N k_B / 2) \ln(3/2)$, is of course just Pauling's original result revamped for the pyrochlore spin ice problem. Another way to obtain the residual entropy is as follows. For a pyrochlore lattice with N spins, there are $N/4$ tetrahedron unit cells. Take all the "upward" tetrahedron unit cells in Fig. 1.2. If all these tetrahedra are in a spin ice state, there can be $6^{N/4}$ independent spin ice configurations in the system. However, not all these states are valid ground states. The $N/4$ "downward" tetrahedra, which are formed by the corners of these upward tetrahedra, must also satisfy the ice rules. The probability that a random tetrahedron satisfies the ice rule is $6/16$; so the above number should be divided by this scale factor for each "downward" tetrahedron, hence giving a total of $6^{N/4} (6/16)^{N/4} = (3/2)^{N/2}$ ice-rule obeying states for the whole system, as obtained above. Finally, one could have also simply directly borrowed Pauling's result. In the mapping from water ice to Anderson's antiferromagnet, or alternatively to spin ice, N oxygen O^{2-} ions correspond to $2N$ spins. We shall now show that this Pauling's estimate, $S_0 = (N k_B / 2) \ln(3/2)$, for spin ices, is in good agreement with experimental results.

1.3.5 Residual entropy of $Dy_2Ti_2O_7$ and $HfO_2Ti_2O_7$

The first compelling thermodynamic evidence for the existence of a spin ice state in Ising pyrochlore systems was obtained via measurements of the magnetic specific heat, $C(T)$, on $Dy_2Ti_2O_7$ [7]. This material with magnetic Dy^{3+} is, as $HfO_2Ti_2O_7$, characterized by a strongly Ising-like ground state doublet that is separated by a large energy of approximately 300 K from the excited doublet. The temperature dependence of $C(T)$ is shown in the upper panel of Fig. 1.3. To determine the residual magnetic entropy of $Dy_2Ti_2O_7$, Ramirez and co-workers followed an approach similar to the one that Giauque and colleagues used to determine the entropy of water ice [2,3].

In general, one can only measure the change of entropy between two temperatures. Giauque and collaborators calculated the entropy change of water between 10 K and the gas phase of H_2O by integrating the specific heat divided by temperature, $C(T)/T$, adding to it the latent heat at the melting and vaporization transitions. They then compared this value with the absolute value expected for the entropy calculated for an ideal (non-interacting) gas phase using inputs from spectroscopic

measurements which allowed to determine the rotational and vibrational energy spectrum, hence the roto-vibrational entropy, and adding to it the translational entropy of an ideal gas given by the Sackur-Tetrode equation. The difference between the measured value and the theoretically expected value gave the residual entropy of water ice, whose origin was explained by Pauling [4].

Ramirez et al. measured the magnetic specific heat of a powder sample of $\text{Dy}_2\text{Ti}_2\text{O}_7$ between $T_1 = 300 \text{ mK}$, "inside" the frozen ice regime, and $T_2 = 10 \text{ K}$, in the paramagnetic regime, where the expected entropy per mole should be $R \ln(2)$ for a two-state system ($R = N_0 k_B$ is the gas molar constant and N_0 is the Avogadro number).

The entropy change between T_1 and T_2 , $S_{1,2}$, was found by integrating $C(T) = T$ between these two temperatures:

$$S_{1,2} = S(T_2) - S(T_1) = \int_{T_1}^{T_2} \frac{C(T)}{T} dT : \quad (1.13)$$

The lower panel of Fig. 1.3 shows that the magnetic entropy recovered is approximately $3.9 \text{ J mol}^{-1} \text{ K}^{-1}$, a value quite a bit smaller than $R \ln(2) = 5.76 \text{ J mol}^{-1} \text{ K}^{-1}$. The difference, $1.86 \text{ J mol}^{-1} \text{ K}^{-1}$ is fairly close to the above Pauling-like estimate for the entropy associated with the extensive degeneracy of ice: $(R/2) \ln(3/2) = 1.68 \text{ J mol}^{-1} \text{ K}^{-1}$, consistent with the existence of an ice-rule obeying spin ice state in $\text{Dy}_2\text{Ti}_2\text{O}_7$. More recent measurements [44] on single crystals of $\text{Dy}_2\text{Ti}_2\text{O}_7$ have found a specific heat below 1.5 K that differs quantitatively fairly significantly from that of Ref. [7], ultimately giving a much better agreement between the experimentally determined residual entropy of the material and Pauling's value.

As discussed above, $\text{Ho}_2\text{Ti}_2\text{O}_7$ was the first material proposed as a spin ice system. It turns out that $\text{Ho}_2\text{Ti}_2\text{O}_7$ is less convenient to perform low temperature specific heat measurements than $\text{Dy}_2\text{Ti}_2\text{O}_7$. The origin of this difficulty stems from the unusually large hyperfine interaction between the nuclear and electronic spins of Ho^{3+} . This interaction leads to a Schottky anomaly in the specific heat at a temperature $T \approx 0.3 \text{ K}$ which significantly obscures the otherwise purely electronic broad specific heat feature arising from the formation of the ice-rule obeying low-energy manifold [45]. Once the nuclear contribution to the specific heat has been subtracted, the exposed electronic contribution and the consequential residual Pauling entropy of the spin ice state in $\text{Ho}_2\text{Ti}_2\text{O}_7$ can be revealed [31, 46].

In summary, the $\text{Ho}_2\text{Ti}_2\text{O}_7$ and $\text{Dy}_2\text{Ti}_2\text{O}_7$ possess a residual low temperature entropy compatible with that estimated on the basis of a Pauling argument applied to the ferromagnetic nearest-neighbor 1111 Ising model on the pyrochlore lattice. The related $\text{Ho}_2\text{Sn}_2\text{O}_7$ [47] and $\text{Dy}_2\text{Sn}_2\text{O}_7$ [48] are also spin ice systems.

1.4 Dipolar Spin Ice Model

1.4.1 Competing interactions in dipolar spin ice model

In Section 1.3.4, we invoked a simple nearest-neighbor ferromagnetic 1111 Ising model to rationalize the spin ice phenomenology in real materials. Yet, it was argued in Section 1.3.2 that magnetic dipole-dipole interactions are often of sizeable strength in rare-earth magnetic systems. In the case of $\text{Dy}_2\text{Ti}_2\text{O}_7$ and $\text{Ho}_2\text{Ti}_2\text{O}_7$,

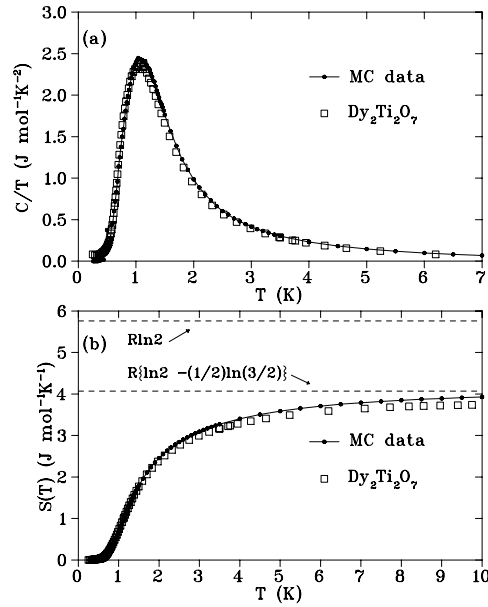


Fig. 1.3. (a) Specific heat and (b) entropy data for $\text{Dy}_2\text{Ti}_2\text{O}_7$ from Ref. [7], compared with Monte Carlo simulation results [30] for the dipolar spin ice model, with $J=3 = 1.24$ K and $5D=3 = 2.35$ K. Two temperature regimes can be identified. (i) At a temperature T much higher than the peak temperature, $T_{\text{peak}} = 1.24$ K, the system is in the paramagnetic regime and is weakly correlated and individual tetrahedra do not obey the "two-in/two-out" ice rules. As the temperature approaches T_{peak} , the ice-rules become progressively fulfilled. The Schottky-like peak in C arises when the temperature drops below the energy gap between the ice-rule obeying states and the excited "three-in/one-out" states and "all-in/all-out" states. (ii) As T drops below T_{peak} , the spin flip rate drops exponentially rapidly [50] as the system settles in an ice-rule obeying state with two spins "in" and two spins "out" on each tetrahedron. There is no phase transition between the high temperature paramagnetic state ($T > T_{\text{peak}}$) and the spin ice regime at $T < T_{\text{peak}}$. The spin ice regime can therefore be described as a collective paramagnet [14]. (Figure reprinted with permission from B. C. den Hertog and M. J. P. Gingras, Phys. Rev. Lett. 84, 3430 (2000). Copyright 2000 by the American Physical Society.)

the value of $D = \frac{1}{4} (g_L \mu_B J_z i)^2 = (4 \mu_{\text{nn}})^2$ is estimated at $D = 1.4$ K [30, 37, 38], which is comparable to the experimentally measured Curie-Weiss temperature θ_{CW} in these materials. Even if one was assuming that the nearest-neighbor exchange $J_{\text{CW}} = 1$ K, one is still in a regime where the dipolar interactions are comparable in magnitude to the nearest-neighbor exchange interactions [7, 30, 37]. This observation raises a paradox. The existence of a ground state with extensive degeneracy should in principle result from the underconstraints that the Hamiltonian imposes on the spin configurations that minimize the classical ground state en-

ergy [16]. Consider the dipolar interactions in Eq. (1.8). First of all, they are rather complicated as they couple spin and space directions via the $(\hat{z}_i - \hat{z}_j)(\hat{r}_{ij} - \hat{r}_{ij})$ term. Secondly, dipolar interactions are very long-ranged, decaying as $1/r_{ij}^3$ with distance r_{ij} separating ions i and j . How can one therefore understand that the dipolar interactions allow for the emergence of an extensively degenerate spin ice state at a temperature T of order of D with spin couplings as "complicated" (i.e. anisotropic and long-range) as the dipolar interactions? How dipolar interactions manage to do so is the "second magic" of dipolar spin ice.

One way to first investigate this question is to go beyond the nearest-neighbor ferromagnetic Ising model and perform Monte Carlo simulations where the dipolar interactions of Eq. (1.8) are taken into account [7,30,31,37,32,33,49,50]. The first studies of this problem considered truncated dipolar interactions beyond a certain cut-off distance [7,37]. It was then followed by another work [30] that incorporated the true long-range dipolar interactions using the so-called Ewald summation method [50] which is commonly used to handle long-range Coulomb and dipolar interactions [51].

Consider $H_{\text{D SM}}$ in Eq. (1.8) with long-range dipole-dipole interactions, $D \neq 0$, and only nearest-neighbor exchange $J_{ij} = J$ as a starting model to describe $\text{Dy}_2\text{Tb}_2\text{O}_7$. One can take the dipolar interaction coupling D as a more or less a priori known quantity if one makes the reasonably accurate approximation that the crystal field ground state doublet is essentially composed of only the $j = 15/2; m_j = 15/2$ components. This gives $D \approx 1.4 \text{ K}$ [30]. Hence, the nearest-neighbor exchange J is the only unknown parameter in the model. In the Monte Carlo simulations [30], it was found that fitting either the height of the specific peak or the temperature at which the peak occurs allows for a unique and consistent determination of J . The values $J = 3.124 \text{ K}$ [30,43] and $J = 3.055 \text{ K}$ [31] were estimated for $\text{Dy}_2\text{Tb}_2\text{O}_7$ [30] and $\text{Ho}_2\text{Tb}_2\text{O}_7$ [31], respectively. Interestingly, the nearest-neighbor interaction J is antiferromagnetic in both cases which should, on its own, and according to the discussion in Section 1.3.4, give rise to a four sublattice long-range Neel ordered phase [30]. This already indicates that it must be the dipolar interactions that are responsible for the spin ice phenomenology. Figure 1.3 shows that a Monte Carlo simulation of the dipolar spin ice model (D SM) in Eq. (1.8), with $J = 3.124 \text{ K}$ and $5D = 3.235 \text{ K}$, gives an excellent description of the magnetic specific heat data $C(T)$ of $\text{Dy}_2\text{Tb}_2\text{O}_7$. Also, as a consequence, the integration of the Monte Carlo $C(T) = T$ reproduces the experimental Pauling-like residual entropy (see lower panel of Fig. 1.3). A similar agreement between experimental and Monte Carlo data for the specific heat was found for $\text{Ho}_2\text{Tb}_2\text{O}_7$ using with $J = 3.055 \text{ K}$ and $5D = 3.235 \text{ K}$ [31]. Furthermore, in $\text{Ho}_2\text{Tb}_2\text{O}_7$, it was possible to perform neutron scattering studies on a single crystal [31]. After having fixed J from $C(T)$ data on $\text{Ho}_2\text{Tb}_2\text{O}_7$, it was found that the scattering wave vector q dependence of the experimental neutron scattering intensity was well reproduced by results from Monte Carlo simulations [31], as illustrated in Fig. 1.4.

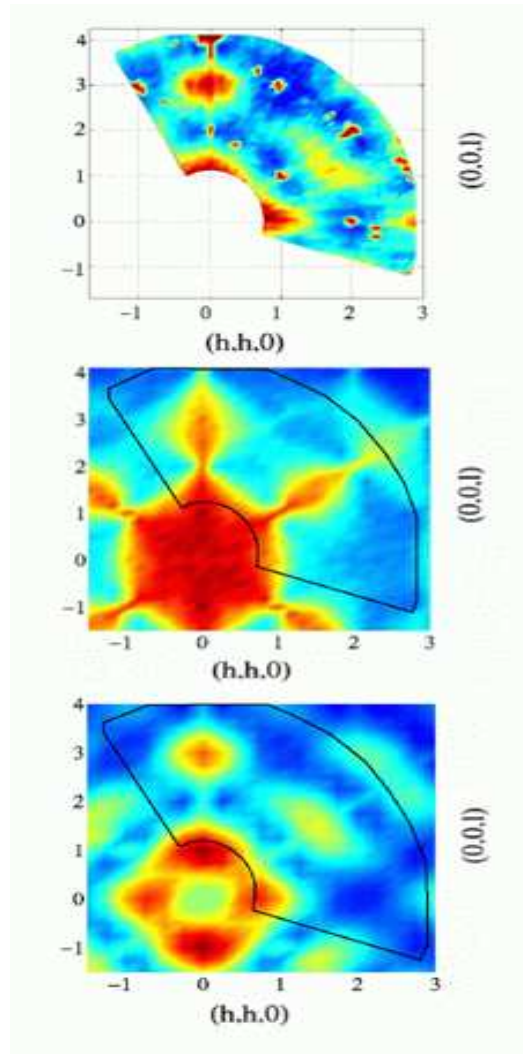


Fig. 1.4. $\text{H}_2\text{Ti}_2\text{O}_7$: Neutron scattering in the (hhl) plane showing experimental data (upper panel; the sharp spots are nuclear Bragg scattering with no magnetic component), compared with Monte Carlo simulations of the near neighbour spin ice model (middle panel) and dipolar model (lower panel) [31]. Blue (light) indicates the weakest and red-brown (dark) the strongest intensity. (Figure reprinted with permission from S. T. Bramwell et al., Phys. Rev. Lett. 87, 047205 (2001). Copyright 2001 by the American Physical Society.)

Hence, despite their complex structure, not only are dipolar interactions compatible with the existence of a degenerate state, but in fact they appear to be responsible for it, since the nearest-neighbor exchange interaction J , being antiferromagnetic in Ho_2TbO_7 and Dy_2TbO_7 , would by itself lead to long range order. Hence, where does the spin ice phenomenology come from in the dipolar spin ice model of Eq. (1.8) with long range dipole-dipole interactions? A first way to address this question is to take the dipolar interactions and truncate them at nearest-neighbor distance. On the pyrochlore lattice, we have $\sum_j \mathbf{r}_{ij}^{-3} = 1/3$ and $(\sum_j \mathbf{r}_{ij}^{-3}) (\sum_j \mathbf{r}_{ij}^{-3}) = 2/3$ for nearest neighbor ions i and j . We thus have

$$H = \sum_{i,j} \frac{J}{3} + \frac{5D}{3} \sum_{i,j} \frac{z_i z_j}{r_{ij}^3} + H_{>r_{nn}}^{\text{dip}} \quad (1.14)$$

where we have incorporated all dipolar interactions beyond nearest-neighbor distance r_{nn} into $H_{>r_{nn}}^{\text{dip}}$.

The first term is therefore that of an effective nearest-neighbor pyrochlore Ising antiferromagnet [13], which is frustrated and possess a Pauling entropy as long as $(J + 5D)/3 > 0$, while a four sublattice "all-in/all-out" long-range Neel order occurs for $(J + 5D)/3 < 0$. Monte Carlo simulations [49,50] and mean-field theory [52] find that $H_{>r_{nn}}^{\text{dip}}$ only slightly modifies the location of the Neel to spin ice boundary from $(J + 5D)/3 = 0$ to $(J + 4.53D)/3 = 0$. In other words, the long range dipole-dipole interactions slightly stabilize the Neel order to the detriment of the spin ice state [30,49,50]. Using the $J=3$ and $5D=3$ values above for Dy_2TbO_7 and Ho_2TbO_7 , we find that both materials fulfill the criterion $(J + 4.53D)/3 > 0$, as well as the less accurate $(J + 5D)/3 > 0$ criterion, in order to be characterized as dipolar spin ice systems.

Having established an "order 0" criterion, $(J + 5D)/3 > 0$, to determine whether a dipolar pyrochlore Ising system exhibits spin ice behavior, we now have a sharp question in hand: how is it that the long range $1/r_{ij}^3$ tail of $H_{>r_{nn}}^{\text{dip}}$ does not (seemingly) lift the extensive degeneracy created by the nearest-neighbor part? To answer this question, we first turn to mean-field theory.

1.4.2 Mean-field theory

The general idea of the Ginzburg-Landau theory is to determine when the paramagnetic phase, where all the components of the local (on-site) magnetization, $m_i^{a,u}$ vanish, become spontaneously unstable (i.e. critical) against the development of nonzero $m_i^{a,u}$. To proceed, we follow here the approach laid out in Refs. [52,53,54]. Consider a general bilinear spin Hamiltonian

$$H = \frac{1}{2} \sum_{(i,j)} S_i^{a,u} K_{uv}^{ab}(i;j) S_j^{b,v} \quad (1.15)$$

where $S_i^{a,u}$ is the $u = x,y,z$ components of spin S_i^a on the a^{th} sublattice of the i^{th} primitive basis and $K_{uv}^{ab}(i;j)$ is a generalized spin-spin interaction. Making the mean-field ansatz

$$(S_i^{a,u} - m_i^{a,u})(S_j^{b,v} - m_j^{b,v}) = 0; \quad (1.16)$$

where $m_i^{a,u}$ is the thermal average $\langle S_i^{a,u} \rangle$, allows to decouple H above and write it as an effective one-particle problem from which the free-energy, F ($\text{fm}_i^{a,u}g$)

$^{-1} \ln(Z)$, where $Z = \text{Trace}[\exp(-H)]$ is the partition function, can be expanded as a Taylor series of the order parameters $m_i^{a;u}$. Here we take $\beta = 1/T$, where T is the temperature and work in units where the Boltzmann constant $k_B = 1$. The leading term in F is quadratic in the $m_i^{a;u}$:

$$F = \frac{1}{2} \sum_{i,j} \sum_{a,b} \sum_{u,v} m_i^{a;u} m_j^{b;v} n T^{-1} K_{uv}^{ab}(i;j) + F_0(T) \quad (1.17)$$

where $F_0(T)$ is a $m_i^{a;u}$ -independent temperature-dependent function and n is the number of spin components of S_i^a . We next introduce the Fourier transform representation of $m_i^{a;u}$

$$m_i^{a;u} = \sum_q m_q^{a;u} e^{i(q \cdot R_i^a)}; \quad (1.18)$$

$$K_{uv}^{ab}(i;j) = \frac{1}{N_{\text{cell}}} \sum_q K_{uv}^{ab}(q) e^{i(q \cdot R_{ij}^{ab})}; \quad (1.19)$$

where N_{cell} is the number of FCC Bravais lattice points, and R_i^a denotes the position of a magnetic ion on sublattice a of basis cell i . Equations (1.18) and (1.19) applied to F give

$$\frac{(F - F_0)}{N_{\text{cell}}} = \frac{1}{2} \sum_q \sum_{a,b} \sum_{u,v} m_q^{a;u} m_q^{b;v} n T^{-1} K_{uv}^{ab}(q) : \quad (1.20)$$

To proceed, a transformation to normal modes is necessary to diagonalize $K_{uv}^{ab}(q)$ via

$$m_q^{a;u} = \sum_{\alpha} U_{u;\alpha}^{a;q}(q) \alpha; \quad (1.21)$$

where the Greek indices $(\alpha;)$ label the normal modes, $\alpha;^i$. $U(q)$ is the unitary matrix that diagonalizes $K_{uv}^{ab}(q)$ in the spin-sublattice space with eigenvector (q) ,

$$U^\dagger(q) K(q) U(q) = \Lambda(q); \quad (1.22)$$

where, in component form, $U_{u;\alpha}^{a;q}(q)$ represents the $(a;u)$ component of the $(\alpha;)$ eigenvector at q with eigenvalue $\Lambda_\alpha(q)$. Therefore, the mean-field free energy, to quadratic order in the normal modes variables, is

$$F(T) = \frac{1}{2} \sum_q \sum_{\alpha} \alpha;^i n T^{-1} \Lambda_\alpha(q) \alpha;^i : \quad (1.23)$$

For the Ising case that interests us, we have $n = 1$ and the indices representing the spin components $(u;v)$ and the label a are dropped from Eq. (1.23). Our main goal is to diagonalize K^{ab} which, by taking a tetrahedron primitive basis with local Ising spins, is now simply a 4×4 matrix, and determine the spectrum $\Lambda(q)$. Let us denote $\Lambda^{\text{max}}(q)$, the largest of the four $\Lambda(q)$ at each q . Let us assume now that the 3-dimensional surface $\Lambda^{\text{max}}(q)$ (as a function of (q_x, q_y, q_z)) reaches an absolute maximum value over the whole Brillouin zone for some q_{ord} , which we

shall label $m_{\text{ax}}(q_{\text{ord}})$. q_{ord} is called the ordering wave vector and $m_{\text{ax}}(q_{\text{ord}})$ is the critical temperature, T_c , because, when the temperature T drops below $m_{\text{ax}}(q_{\text{ord}})$, $(T - m_{\text{ax}}(q_{\text{ord}}))$ in Eq. (1.23) changes sign, causing the mode $m_{\text{ax}}(q_{\text{ord}})$ to go soft (i.e. critical) and to develop a nonzero thermal expectation value, at least according to mean-field theory. A key property of highly frustrated systems, such as the classical Heisenberg antiferromagnet on pyrochlore, kagome and face-centered cubic lattices, is that an infinitely large number of modes go soft/critical simultaneously at T_c [53].

For the 1111 nearest-neighbor Ising pyrochlore ferromagnet (1st term on the right hand side of Eq. (1.14)), or Anderson's pyrochlore Ising antiferromagnet, one finds that there are two exactly degenerate branches of soft modes that have an identical eigenvalue $m_{\text{ax}}(q)$ for each wave vector q in the Brillouin zone (see Fig. 1.5). This result is obtained after constructing the 4×4 $K^{ab}(q)$ matrix obtained from Eq. (1.19) and finding its 4 eigenvalues. The mean-field theory of the nearest-neighbor model therefore predicts, via a reciprocal space description, that there is no unique ordering wavevector q_{ord} developing at T_c . In fact, there are $2N_{\text{cell}}$ modes (i.e. an extensive number of modes) that go soft simultaneously at $T_c = 2(J=3 + 5D=3)$, where $N_{\text{cell}} = N/4$ is the number of primitive basis cells, and N is the number of magnetic moments. This result agrees with the discussion that the nearest-neighbor spin ice model has a degenerate ground state.

What about the role of the long range dipole-dipole interactions beyond nearest neighbors contained in $H_{>\text{nn}}^{\text{dip}}$ in Eq. (1.14)? Since we are still only considering an Ising model, the 4×4 $K^{ab}(q)$ matrix is merely constructed by adding the Fourier transform of $H_{>\text{nn}}^{\text{dip}}$. Because of the long-range $1/r_{ij}^3$ nature of the dipolar interactions, it is somewhat technical to proceed with the calculation of the Fourier transform in Eq. (1.19) [54,55]. The simplest, although not well controlled way to do so, is to truncate $H_{>\text{nn}}^{\text{dip}}$ at some cut-off distance R_c and determine $m_{\text{ax}}(q_{\text{ord}})$ for that R_c [52]. One can then monitor the evolution of the $m_{\text{ax}}(q)$ "surface" and the corresponding q_{ord} with progressively increasing R_c . For "small" R_c , say R_c less than the tenth nearest-neighbor distance, one finds that $m_{\text{ax}}(q)$ acquires sizeable dispersion and a q_{ord} is selected. However, the value of q_{ord} depends on the chosen value of R_c , a physically unacceptable result given that ultimately $R_c = \infty$ must be considered [52]. As R_c is pushed to larger and larger value, $m_{\text{ax}}(q)$ becomes progressively less dispersive with a q_{ord} moving towards 001. This result is confirmed by calculations of $K^{ab}(q)$ directly in q space using the Ewald-summation method [56]. Figure 1.5 shows the q dependence of $m_{\text{ax}}(q)$ in the (hhl) reciprocal plane.

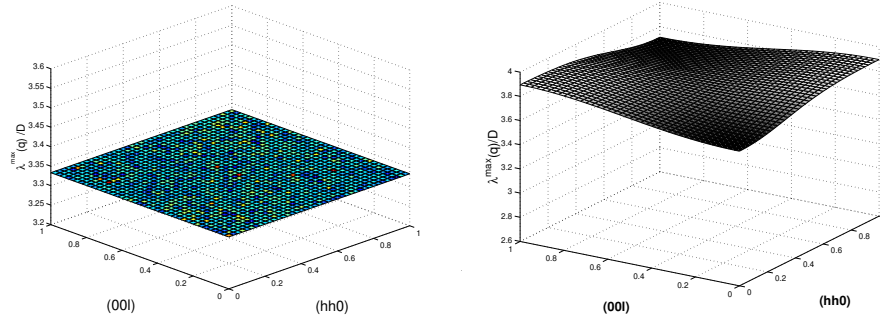


Fig. 1.5. Left: spectrum of $\chi^{\text{max}}(\mathbf{q}) = D$ for an effective nearest-neighbor spin ice model where the dipole-dipole interactions are truncated at nearest-neighbor distance. The spectrum is flat and there is no selected ordering wave vector \mathbf{q}_{ord} . Since there is one net uncompensated spin out of the three spins neighboring a reference spin on a given tetrahedron, the net "mean-field" acting at a site is twice the effective nearest-neighbor interaction for the Ising variable, i.e. $5D = 3$. Hence, the mean-field T_c is $10D = 3 \times 3.33$ corresponding here to the q-independent $\chi^{\text{max}}(\mathbf{q})$. Right: $\chi^{\text{max}}(\mathbf{q}) = D$ for the full dipolar spin ice model with $J_{ij} = 0$ in Eq. (1.8). Note the slightly dispersive nature of $\chi^{\text{max}}(\mathbf{q}) = D$ which displays a maximum at $\mathbf{q}_{\text{ord}} = 001$.

One interpretation of the above mean-field theory calculation is that there exists a sort of self-screening in place such that the selection of an ordering wave vector \mathbf{q}_{ord} from progressively increased cut-off radius R_c cancels the ordering "promoted" by shells of spins of smaller radii. However, this is an incomplete description of what really is the microscopic reason as to why the dipolar interactions give rise to a fulfillment of the ice rules. In other words, why does dipolar spin ice obeys the ice rules [55]? We return to this question in Section 1.4.4. Let us for the moment just take the results of the mean-field calculations at face value. These show that the ultimate selection of a \mathbf{q}_{ord} is "fragile" in the dipolar spin ice model. By "fragile", we refer to the flatness of the spectrum of $\chi^{\text{max}}(\mathbf{q})$ which shows that dipolar spin ice has very little propensity to select an ordered state. Indeed, a slight modification of the exchange interactions beyond nearest-neighbors in Eq. (1.8) can dramatically alter the spin-spin correlations in the spin ice regime [33]. Yet, as mentioned above, a careful consideration of $\chi^{\text{max}}(\mathbf{q})$ does reveal that there is an absolute maximum of $\chi^{\text{max}}(\mathbf{q})$ at $\mathbf{q}_{\text{ord}} = 001$. In other words, dipolar spin ice is characterized by an ordered phase with a unique commensurate propagation wave vector and that, as the system is cooled down from the paramagnetic phase, it should undergo a phase transition to a long-range ordered ground state with no extensive degeneracy. Since this is a classical system, quantum fluctuations cannot inhibit the development of long-range order as occurs in systems such as described in other chapters of this book. Mean-field theory alone "saves" the third law of thermodynamics for the dipolar spin ice model without having to invoke the effects of quantum mechanics at low temperature.

What happens to this predicted long-range ordered phase in both the Monte Carlo simulations of the dipolar spin ice model and in real systems? It is easier to first address this question in the case of the simulations, as we do in the next section.

1.4.3 Loop Monte Carlo simulations and phase diagram of dipolar spin ice

In Monte Carlo simulations that employ simple conventional Metropolis single spin flip dynamics [30,31], the rate of accepted spin flips dies off exponentially fast with decreasing temperature once the system has entered the spin ice regime where the "two-in/two-out" ice rules are strictly obeyed [50]. For example, in simulations of $\text{Dy}_2\text{Tb}_2\text{O}_7$, one finds that it becomes for all practical purposes essentially impossible to equilibrate the system below a "freezing temperature" T_f around 0.4 K [50]. Interestingly, this temperature more or less corresponds to the freezing temperature found in AC susceptibility measurements on $\text{Dy}_2\text{Tb}_2\text{O}_7$ [57]. One can then re-interpret the results of mean-field theory in the light of the Monte Carlo results. The flatness of $\chi^{\text{max}}(q)$ illustrates the competition between all the quasi-degenerate ice-rule obeying quasi-critical modes that exist in the dipolar spin ice model. In real space, once the system is cooled into the ice regime, that is below a temperature at which the specific heat peaks (see top panel in Fig. 1.3), it becomes extremely difficult to flip spins that would violate the ice rules when the temperature is much lower than the energy barrier of approximately $2(J=3 + 5D=3)$. Hence, while the low temperature spin dynamics within the spin ice state is extremely sluggish, the system has not yet reached the critical temperature to long-range order. The spin ice state, or regime, must therefore be seen as smoothly connected with the high temperature paramagnetic phase. In other words, the spin ice state is a paramagnetic state, a collective paramagnetic state to be more precise and to borrow Villain's terminology [14]. That is, spin ice is a classical spin liquid, albeit with extraordinarily slow spin dynamics. One is therefore led to ask a number of questions: How can the out-of-equilibrium freezing of spin ice be beaten, at least within a computational attack on the dipolar spin ice model? What is the long-range ordered phase, what is the nature of the phase transition and at what temperature does it ultimately occur?

In order to explore the low temperature ordering properties of dipolar spin ice, one needs a Monte Carlo algorithm with non-local updates that effectively bypass the energy barriers that separate nearly degenerate states and allows the simulation to explore the restricted ice-rules phase space that prevents ordering in the model [49,50]. One first identifies the true zero energy modes that can take the near-neighbor spin ice model from one ice state to another exactly energetically degenerate ice state. An example of these zero modes, or loops, is shown in Fig. 1.2. With interactions beyond nearest-neighbor, these "loop moves", where spins are flipped on closed loops without violating the ice rules, become quasi-zero modes that can take the dipolar spin ice model from one ice-rules state to another without introducing ice-rule defects into the tetrahedra. This allows all of the quasi-degenerate spin ice states to be sampled ergodically, and facilitates the development of a long-range ordered state at low temperatures. The algorithm used to identify loops of "potentially flipable spins" is described in Refs. [49,50,58,59]. Once a loop has been identified, the energy difference, between the original spin configuration for that loop and the one with flipped spins, which is due to the long-range part of the dipolar interactions, is calculated. The flipping of the spins on the loop is then decided upon according to a standard Metropolis test. From the loop Monte Carlo simulations [49,50], one finds, for $J=3 = 1.24 \text{ K}$ and $5D=3 = 2.35 \text{ K}$, a sharp first order transition at $T_c = 180 \text{ mK}$, or $T_c/D = 0.128$ (see Fig. 1.6). A detailed analysis reveals several properties at the transition [49,50]:

1. The transition is an extremely strong first order transition.
2. The entropy removed on the high and low temperature "wings" of the transition plus the latent heat associated with the transition equals Pauling's residual entropy within 1%–2%.
3. The state below T_c is a long-range ordered ice-rules obeying state and is identical to the one predicted by mean-field theory [52,56].
4. T_c is independent of $D=J$, with $T_c=D=0.128$.

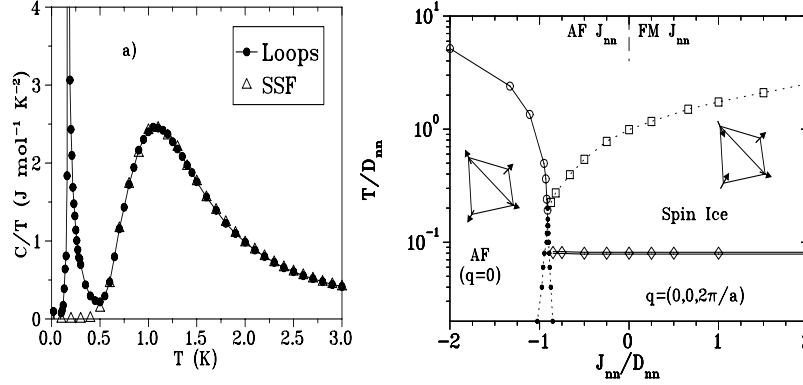


Fig. 1.6. Results from loop Monte Carlo simulations. Left: the low temperature magnetic specific heat for a system size $L = 4$ and for $J=3 = 1.24$ K and $5D=3 = 2.35$ K values for $Dy_2Ti_2O_7$. Closed circles are simulation data using loop Monte Carlo simulations [49,50]. Open triangles are data obtained using standard single spin flip Metropolis algorithm [30]. Right: Phase diagram of the dipolar spin ice model with $J_{nn} = J=3$ and $D_{nn} = 5D=3$. The antiferromagnetic four sublattice Néel ground state is with "all-spins-in/all-spins-out" configuration for each tetrahedron. The spin ice configuration, which includes the $q = (0;0;2\pi/a)$ ground state, is a "two spins in/two spins out" configuration for each tetrahedron [49,50]. The region encompassed between the quasi-vertical dotted lines displays hysteresis in the long-range ordered state selected ($q = 0$ vs. $q = (0;0;2\pi/a)$) as $J_{nn}=D_{nn}$ is varied at fixed temperature T .

One can now return to the question asked earlier: "What happens to the numerically predicted phase transition to long-range order in real systems?" The numerical evidence for a first order transition to long-range order in the dipolar spin ice model is compelling [49,50]. However, there has so far not been any reported experimental evidence for a phase transition in either $Dy_2Ti_2O_7$ [57] or $H_2O_2Ti_2O_7$ [6,9] down to approximately 60 mK. A possible, if not likely, reason for this failure of real spin ice materials to develop long range order at low temperature is that the spins in real materials are frozen and cannot thermally equilibrate since real systems "do not benefit" from the non-local type of spin dynamics such as the one employed in loop Monte Carlo simulations. Another possibility [33] is that perturbative J_{1j} exchange interactions beyond nearest-neighbor in Eq. (1.8) frustrates the development

of the long range order discussed above, pushing T_c below the lowest temperature considered so far in experiments [57].

Before we briefly discuss in the last section of this chapter some avenues of research currently pursued in experimental studies of spin ices and related materials, we revisit the question of the microscopic origin of the ice rules in the dipolar spin ice model.

1.4.4 Origin of ice rules in dipolar spin ice

The Monte Carlo simulation results of Section 1.4.1 show that the spin ice phenomenology is due to long-range dipolar interactions. The mean-field theory calculations of Section 1.4.2 provide a first clue as to the mechanism behind the formation of the ice rules. However, neither method really explains why the dipolar spin ice obeys the ice rules. A successful approach to answer this question was reported in Ref. [55].

The first important ingredient [60] is to note that the "two-in/two-out" ice rules on the pyrochlore lattice,

$$\sum_{i=1}^4 s_i = 0; \quad (1.24)$$

where the sum is carried over up and down tetrahedra, is equivalent to a divergence-free "spin field" \mathbf{B} , $\nabla \cdot \mathbf{B} = 0$. These "lattice flux" are link variables that "live" on the diamond lattice dual to the pyrochlore lattice and ∇ is the lattice divergence. By introducing a weight $\mathcal{B}(\mathbf{r})$ for nonzero flux (locally broken ice rules) of the form

$$\mathcal{B}(\mathbf{r}) \propto \exp \left[-\frac{K}{2} \int d^3x \mathcal{B}(\mathbf{r})^2 \right]; \quad (1.25)$$

one can solve for the correlations

$$\langle \mathcal{B}_u(0) \mathcal{B}_v(x) \rangle \propto \frac{3x_u x_v - r_{uv}^2}{r^5} \quad (1.26)$$

where u, v are cartesian components. Equation (1.26) reveals that the local constraint, the ice rules, lead to spin-spin correlations that are dipolar-like at large distance.

The second important observation [55] is that one can construct a spin-ice-like toy model whose eigenmodes ϕ_q can be used to form a projector onto the ice-rule obeying ground states. Because of the asymptotic dipolar-like correlations that ice-rules obeying ground state possesses, according to Eq. (1.26), the real space matrix elements of this projector turns out to be the same as the dipolar part of the interactions (the second term) in H_{DSM} plus a small rapidly ($1/r_{ij}^5$) converging correction term, $V_{ab}(r_{ij})$. In other words, the dipolar interactions between the magnetic moments is, up to a small rapidly decaying short-range corrections, a projector onto all possible ice-rule ground states. Hence, as a dipolar Heisenberg system is cooled down below a temperature of the order of D , the spin configurations get energetically forced onto an ice-rule state, almost indiscriminately initially, when $V_{ab}(r_{ij}) < T < D$. However, ultimately, the temperature reaches the scale of $V_{ab}(r_{ij})$ and a transition to a long-range ordered spin ice state, the one discussed in Section 1.4.3, occurs, provided ergodicity can be maintained [49, 50].

A possibly much simpler explanation has recently been proposed [61]. "Exploding" each point dipole into its constitutive magnetic (monopole) charges, and imposing that each tetrahedron unit cell is neutral (magnetic charge wise), automatically leads to the conclusion that all ice-rule obeying states are, again up to a small rapidly decaying short-range correction, a ground state of the microscopic magnetostatic dipolar interactions of Eq. (1.8) [61]. Those magnetic charges interact as $1/r$ for large inter-charge separation r . Magnetic field driven [61] and temperature driven [62] nucleation of those objects has been invoked to explain thermodynamic [61] and dynamical [62] properties of spin ice materials. We discuss below their possible experimental manifestation.

1.5 Current Research Topics in Spin Ices and Related Materials

Since the discovery of spin ice behavior in $\text{Ho}_2\text{Ti}_2\text{O}_7$ [5] and $\text{Dy}_2\text{Ti}_2\text{O}_7$ [7], there has been a flurry of research activities aimed at exploring the interesting thermodynamic and magnetic phenomena offered by spin ices and closely related systems. We briefly review in this section some of the topics that are of current interest in the field of spin ice research.

1.5.1 Magnetic field effects

Because of the large magnetic moment of Dy^{3+} and Ho^{3+} in spin ice materials, even moderately small magnetic field can induce dramatic effects. Of particular interest is the "pinning" of the spins by a sufficiently strong field on one [61,63,64,65], two [32], three [32,66] or the four [67] sites of a primitive tetrahedron cell, depending of the field orientation. This gives rise to interesting collective behaviors such as phase transitions to long range order [32,66], topological Kasteleyn transitions [63,65,67], magnetization plateau states [61,63] and a sort of magnetic monopole gas-liquid transition [61]. We briefly discuss some of the salient features characterizing the behavior of the system according to the direction of the magnetic field, B .

Field along $[\bar{1}12]$, $[\bar{1}1\bar{2}]$, $[\bar{1}\bar{1}2]$, [112]

The case of a very strong B along $\hat{x} + \hat{y} + \hat{z}$ (e.g. [112] direction) with $\mu_B \ll k_B T$ (e.g. [110]) is perhaps the simplest one from the point of view of field-induced collective behavior in dipolar spin ice systems [32]. For B in that direction, the magnetic moments on sublattice #1 with Ising easy-axis direction $\hat{z}_1 = \frac{1}{3}(\hat{x} + \hat{y} + \hat{z})$ (see Section 1.3.2) are perpendicular to B and are therefore decoupled from it. The moments on the three other sublattices are frozen (pinned) in a "one-in/two-out" configuration by a strong B in that direction. In the limit $\beta J \gg 1$, the field-decoupled moments on sublattice #1, which form a regular FCC lattice, are left to interact among themselves via dipolar and exchange interactions at and beyond third nearest-neighbor distances. Numerical simulations [32] and experiments [66] find that, because of those interactions, the field-decoupled moments undergo a phase transition to a ferromagnetic state in $\text{Dy}_2\text{Ti}_2\text{O}_7$ at approximately 0.3 K.

Field along [110]

The situation where B is along [110] is a special case of the above $[\hat{x}; \hat{y}; \hat{z}]$ field direction. For B along [110], moments on sublattices # 1 and # 2, with $\hat{z}_1 = \frac{1}{\sqrt{3}}(\hat{x} + \hat{y} + \hat{z})$ and $\hat{z}_2 = \frac{1}{\sqrt{3}}(-\hat{x} - \hat{y} + \hat{z})$, are decoupled from B . At the same time, the moments on sublattice # 3 and # 4, with $\hat{z}_3 = \frac{1}{\sqrt{3}}(\hat{x} + \hat{y} - \hat{z})$ and $\hat{z}_4 = \frac{1}{\sqrt{3}}(-\hat{x} - \hat{y} - \hat{z})$, are pinned by a strong [10] field. The pyrochlore lattice can be viewed as two sets of perpendicular chains, each set made of, respectively, by the (# 1, # 2) sublattices, which form the so-called \hat{z} chains, and the (# 3, # 4) sublattices, which form the \hat{y} chains [68]. Here, one theoretically expects that the field-decoupled spins on the \hat{z} chains to undergo a collective phase transition, again driven by dipolar and exchange interactions at and beyond third nearest-neighbor distance [32, 69]. Results from specific heat [68] and neutron scattering measurements [5, 40, 70] provide evidence that strong correlations develop among spins on the \hat{z} chains for even a moderate [110] field $B \approx 0.5$ T. However, in contrast to theoretical predictions, no experiment has yet found true long range order among the \hat{z} chains. Numerical [50] and experimental [70] evidence suggests that this failure to observe true long range order may be due to small field misalignments away from perfect [110]. Such an offset in the field direction may be sufficient to frustrate the three-dimensional correlations among \hat{z} chains, causing the system to remain in a quasi-one-dimensional short range state and failing to develop long range order.

Field along [111]

The pyrochlore lattice can also be viewed as an assembly of stacked kagome lattice planes (i.e. planes of corner-shared triangles) separated by a triangular plane above and below each kagome plane such that each triangle is decorated with spins alternatively above and below the kagome plane to give "up" and "down" tetrahedra. At sufficiently low temperature, for a magnetic field B along [111], the apical moments on each tetrahedron point along the field. That is, if B is "up", then spins point "out" on the "up" tetrahedra and "in" in the "down" tetrahedra. For B less than a critical field value, B_c of order of 1 T for $\text{Dy}_2\text{Ti}_2\text{O}_7$ [71] and 1.7 T for $\text{Ho}_2\text{Ti}_2\text{O}_7$ [46, 65], the moments on the kagome plane can still maintain ice-rule obeying configurations "in-in-out" or "in-out-out" on "up" and "down" tetrahedron, respectively. This leaves an intra-tetrahedron degree of freedom associated to the kagome planes (the apical moments are polarized by the field) analogous to that in Pauling's model which, therefore, possess a residual zero point entropy. As long as $B < B_c$, this state with residual entropy, referred to as kagome ice, is characterized by a field-independent [111] magnetization plateau [46, 63, 71]. The magnetic entropy has been predicted [63] and experimentally [72] found to be non-monotonic as a function of B and to exhibit a spike at B_c . Very recent work interprets the transition from the plateau regime to the high field saturated magnetization regime above B_c as a condensation of magnetic monopole like defects [61]. For $B < B_c$, the available degrees of freedom that live on the kagome planes can be mapped to hard core dimers on a honeycomb lattice. Using this description, the kagome ice state is found to be critical. Theory predicts that a tilting of the magnetic field away from perfect [111] alignment allows to control the entropy of this critical state, which is ultimately terminated for a tilting angle above a critical value by a topological phase transition

called Kasteleyn transition [63]. Neutron scattering intensity data on $\text{Ho}_2\text{T}_{1/2}\text{O}_7$ subjected to a magnetic field tilted away from $[111]$ have been compellingly interpreted in terms of such a Kasteleyn transition out of a critical kagome ice state [65].

Field along $[100]$

A field B along $[100]$ has an equal projection along each of the \hat{z}_i Ising easy axis. A field B larger than 0.04 T overwhelms the correlations caused by the long range magnetostatic dipolar interactions and gives rise to a polarized state along $[100]$ that satisfies the ice rules [50]. On the basis of Monte Carlo simulations, it was first believed that for a field less than a critical value, the system undergoes a first order liquid-gas transition between a state of low $[100]$ magnetization to a state with higher $[100]$ magnetization upon cooling [73]. However, a more recent study shows that this problem is more subtle [67]. Indeed, at low temperature, the approach to the saturated magnetization is another example of a Kasteleyn transition which is topological in nature since the magnetization can only be changed via correlated spin excitations that span the whole system. Comparison of simulation data with thermodynamic field dependence of the $[100]$ magnetization for $\text{Dy}_2\text{T}_{1/2}\text{O}_7$ does provide good evidence that the physics of the Kasteleyn transition is indeed at play [67].

1.5.2 Dynamical properties and role of disorder

Experiments have been carried out to investigate and unravel the nature of the persistent spin dynamics observed down to the lowest temperature [76,77,78]. The substitution of the magnetic Ho^{3+} and Dy^{3+} ions by non-magnetic ions affects the spin dynamics and lead to a partial and non-monotonous lifting of the ground state degeneracy [44]. Yet, the interesting problem of the ultimate transition from spin ice to dipolar spin glass as the magnetic rare earth ion is substituted by Y^{3+} has not yet been explored. The origin of the spin dynamics in spin ices is not fully understood [78]. Recent work on $\text{Ho}_2\text{T}_{1/2}\text{O}_7$ proposes that the excitation of nuclear states perturb the electronic Ising spin states and give rise to persistent spin dynamics [79]. A rather interesting aspect of the spin dynamics in spin ice materials, such as $\text{Dy}_2\text{T}_{1/2}\text{O}_7$, is the field temperature, T , independent relaxation rate $\tau(T)$ between 4 K and 13 K [74,75]. This temperature independent regime had previously been interpreted in terms of quantum mechanical tunneling of the spins between their "in" and "out" directions. However, recent work suggests that the magnetic relaxation can be entirely interpreted in terms of the diffusion of thermally-nucleated topological defects, again akin to magnetic monopoles, on trajectories constrained to lie on a network of "Dirac strings" [62].

1.5.3 Beyond the dipolar spin ice model

The large number of high quality experiments on spin ices are now permitting to refine the spin Hamiltonian and extract the exchange interactions beyond nearest-neighbors, allowing an excellent quantitative description of many bulk measurements and neutron scattering experiments [33,64]. In particular, exchange interactions beyond nearest-neighbors are argued to induce weak spin-spin correlations that are responsible for the neutron scattering intensity spanning the Brillouin zone boundaries [33].

1.5.4 Metallic spin ice

The metallic $\text{Pr}_2\text{Ir}_2\text{O}_7$ pyrochlore material exhibits interesting Kondo-like effects with a logarithmic increase of the resistivity and magnetic susceptibility at low temperatures [80,81]. One expects Pr^{3+} in $\text{Pr}_2\text{Ir}_2\text{O}_7$ to be well described by an Ising spin, for which Kondo physics is not straightforwardly explainable. Furthermore, the predominant Pr^{3+} - Pr^{3+} interactions in metallic $\text{Pr}_2\text{Ir}_2\text{O}_7$ would naively be expected to be RKKY-like. In contrast to experimental findings, Monte Carlo simulations on RKKY-coupled Heisenberg spins find a transition to long range order at a temperature of the order of the Curie-Weiss temperature [82]. Hence it is not really clear what is, if any, the role of magnetic frustration in determining the exotic transport and thermodynamic properties of $\text{Pr}_2\text{Ir}_2\text{O}_7$.

1.5.5 Artificial spin ice

Lithographically fabricated single-domain ferromagnetic islands can be arranged such that the magnetic dipolar interactions create a two-dimensional analogue to spin ice. The magnetic moments can be directly imaged, allowing to study the local accommodation of frustration and emergence of ice-rules [83,84]. Also, it has been proposed that a colloidal version of artificial ice can be realized using optical trap lattices [85]. It will be interesting to see more such artificial systems becoming available. The out-of-equilibrium properties of the lithographically made systems subject to nonzero magnetic field promise to be quite interesting.

1.5.6 Stuffed spin ice

One can chemically alter $\text{Ho}_2\text{Ti}_2\text{O}_7$ spin ice by "stuffed" extra Ho^{3+} magnetic moments into the normally non-magnetic Ti sites [86,87]. The resulting series, $\text{Ho}_2(\text{Ti}_{1-x}\text{Ho}_x)_2\text{O}_7$ displays an increased connectivity compared to the standard pyrochlore, making interesting the question as to how the Pauling entropy of "normal" spin ice evolves with stuffing [86,88]. At this time, the question of homogeneity of stuffed spin ice materials remains to be ascertained and more work remains to be done on these systems.

1.5.7 Quantum mechanics, dynamics and order in spin ices

The $\text{Tb}_2\text{Ti}_2\text{O}_7$ [25,26] and $\text{Tb}_2\text{Sn}_2\text{O}_7$ [26] should both possess an Ising ground state doublet, similarly to their Ho and Dy counterpart [24]. However, $\text{Tb}_2\text{Ti}_2\text{O}_7$ remains in a collective paramagnetic (spin liquid) state down to 50 mK despite an antiferromagnetic Curie-Weiss temperature of -14 K [19,25] and is seemingly not a spin ice state [23]. On the other hand, neutron scattering [39] finds a long-range ordered spin ice configuration in $\text{Tb}_2\text{Sn}_2\text{O}_7$, although muon spin relaxation studies find significant spin dynamics in this compound [89,90,91]. What is the role of the deviation from a strictly Ising like description of the magnetic moments in these two materials and the consequential quantum fluctuations is an interesting question that is not yet resolved [23]. In that context, it is interesting to note that the $\text{Pr}_2\text{Sn}_2\text{O}_7$ pyrochlore material has been proposed to display a "dynamical spin ice state" [92]. Little is known about the microscopic physics at play in this system.

1.6 Conclusion

Spin ice materials were discovered just over ten years ago. Since then, their experimental and theoretical investigations have raised many interesting questions regarding several aspects of the physics of frustrated magnetic systems. At the same time, the study of spin ices have led to an enhanced global understanding of many fundamental issues pertaining to frustration in condensed matter systems. Yet, there are still several unanswered questions, in particular in the context of low-temperature spin dynamics, random disorder and properties of metallic Ising pyrochlore systems. These will likely continue to attract attention for many years to come.

1.7 Acknowledgements

I thank Steve Bramwell, Benjamin Canals, Adrian Del Maestro, Byron den Hertog, Sarah Dunsiger, Matt Entezari, Tom Fennell, Jason Gardner, Bruce Gaulin, John Greedan, Ying-Jer Kao, Roger Melko, Hamid Molaian, Jacob Ruess and Taras Yavorskii for their collaboration on projects related to spin ice. I acknowledge many useful and stimulating conversations over the past few years with Tom Devereaux, Rob Hill, Rob Kiehl, Jan Kycia, Chris Henley, Peter Holdsworth, Graeme Luke, Paul McLarty, Roderich Moessner, Jeremy Quilliam, Peter Schier, Andreas Sorge, Kamming Tam, Olek Tchemyshyov and Jordan Thompson. Funding from the NSERC of Canada, the Canada Research Chair Program, the Research Corporation, the Canadian Institute for Advanced Research, the Ontario Innovation Trust, the Ontario Challenge Fund and Materials and Manufacturing Ontario is gratefully acknowledged. The hospitality of the Kavli Institute of Theoretical Physics (KITP) at the University of California of Santa Barbara, where part of this review was written, is acknowledged. Work at the KITP was supported in part by the National Science Foundation under Grant No. NSF PHY 05-51164.

References

1. G. H. Wannier, *Phys. Rev.* **79**, 357 (1950); erratum *Phys. Rev.* **B 7**, 5017 (1973)
2. W. F. Giauque, M. F. Ashley, *Phys. Rev.* **43**, 81 (1933)
3. W. F. Giauque, J. W. Stout, *J. Am. Chem. Soc.* **58**, 1144 (1936)
4. L. Pauling, *J. Am. Chem. Soc.* **57**, 2680 (1935)
5. M. J. Harris, S. T. Bramwell, D. F. McMorrow, T. Zeiske, K. W. Godfrey, *Phys. Rev. Lett.* **79**, 2554 (1997)
6. M. J. Harris, S. T. Bramwell, T. Zeiske, D. F. McMorrow, P. J. C. King, J. Magn. Mater. **177**, 757 (1998)
7. A. P. Ramirez, A. Hayashi, R. J. Cava, R. Siddharthan, *Nature* **399**, 333 (1999)
8. S. T. Bramwell, M. J. P. Gingras, *Science* **294**, 1495 (2001)
9. S. T. Bramwell, M. J. P. Gingras, P. C. W. Holdsworth, in: *Frustrated Spin Systems*, ed. by H. T. Diep (World Scientific Publishing, Singapore, 2004). p.367
10. J. D. Bernal, R. H. Fowler, *J. Chem. Phys.* **1**, 515 (1933)

11. J. M . Ziman, Models of Disorder: The Theoretical Physics of Homogeneously Disordered Systems, (Cambridge University Press, Cambridge, 1976)
12. J. F. Nagle, J. Math. Phys. 7, 1484 (1966)
13. P. W . Anderson, Phys. Rev. 102, 1008 (1956)
14. J. Villain, Z. Phys. B 33, 31 (1979)
15. J. N . Reimers, Phys. Rev. B 45, 7287 (1992)
16. R. Moessner, J. T. Chalker, Phys. Rev. B 58, 12049 (1998)
17. J. E. G reedan, J. of Materials Chemistry 11, 37 (2001)
18. J. S. Gardner, M . J. P. G ingras and J. E. G reedan, to appear in Rev. Mod. Phys. (2009)
19. J. S. Gardner, S. R. D unsiger, B. D. Gaulin, M . J. P. G ingras, J. E. G reedan, R. F. Kie , M . D. Lumsden, W . A. MacFarlane, N . P. Raju, J. E. Sonier, I. Swainson, Z. Tun, Phys. Rev. Lett. 82, 1012 (1999)
20. J. E. G reedan, M . Sato, Y. Xu, F. S. Razavi, Solid State Comm un. 59, 895 (1986)
21. B. D. Gaulin, J. N . Reimers, T. E. Mason, J. E. G reedan, Z. Tun, Phys. Rev. Lett. 69, 3244 (1992)
22. Y. Taguchi, Y. Ohara, H. Yoshizawa, N. Nagaosa, Y. Tokura, Science 291, 2573 (2001)
23. H. R. M olavian, M . J. P. G ingras, B. Canals, Phys. Rev. Lett. 98, 157204 (2007)
24. S. Rosenkranz, A. P. Ramirez, A. Hayashi, R. J. Cava, R. Siddharthan, B. S. Shastry, J. Appl. Phys. 84, 5914 (2000)
25. M . J. P. G ingras, B. C. den Hertog, M . Faucher, J. S. Gardner, S. R. D unsiger, L. J. Chang, B. D. Gaulin, N . P. Raju, J. E. G reedan, Phys. Rev. B 62, 6496 (2000)
26. I. M irebeau, P. Bonville, M . H ennion Phys. Rev. B 76, 184436 (2007)
27. A. Abragam , B. Bleaney, Electron Param agnetic Resonance of Transition Ions, (Dover, 1986)
28. I. D. Ryabov, J. Magn. Reson. 140, 141 (1999)
29. C. Rudowicz, C. Y. Chung, J. Phys.: Condens. Matter 16, 1 (2004)
30. B. C. den Hertog, M . J. P. G ingras, Phys. Rev. Lett. 84, 3430 (2000)
31. S. T. Bram well, M . J. Harris, B. C. den Hertog, M . J. P. G ingras, J. S. Gardner, D. F. M cM orrow , A. R. Wildes, A. L. Cornelius, J. D. M . Champion, R. G . M elko, T. Fennell, Phys. Rev. Lett. 87, 047205 (2001)
32. J. P. C. Ru , R. G . M elko, M . J. P. G ingras, Phys. Rev. Lett. 95, 097202 (2005)
33. T. Yavors'kii, T. Fennell, M . J. P. G ingras, S. T. Bram well, Phys. Rev. Lett. 101, 037204 (2008)
34. S. H. Cumoe, Phys. Rev. B 78, 094418 (2008)
35. P. A. M cClary, S. H. Cumoe, M . J. P. G ingras, J. Phys.: Conf. Ser. 145, 012032 (2009)
36. As a realistic gure of comparison between the spin-spin interactions and H_{cf} , the coupling constants J_{ij} and D should be multiplied by the relevant products of matrix elements. Taking as a rough estimate for such products their magnitude squared of J , $\langle j^2 \rangle \approx 60$ for both Dy^{3+} with $J=15/2$ and Ho^{3+} with $J=8$, we still have $J_{ij} \langle j^2 \rangle$ and $D \langle j^2 \rangle$
37. R. Siddharthan, B. S. Shastry, A. P. Ramirez, A. Hayashi, R. J. Cava and S. Rosenkranz, Phys. Rev. Lett. 83, 1854 (1999)

38. However, in Ref. [33], D was estimated using the crystal field ground state doublet wave functions. This gives a moment $= g_L \mu_B h J_z i$ slightly less than $10 \mu_B$
39. I. Mirebeau, A. Apetrei, J. Rodriguez-Carvajal, P. Bonville, A. Forget, D. Colson, V. Glazkov, J. P. Sanchez, O. Isnard, E. Suard, Phys. Rev. Lett. 94, 246402 (2005)
40. T. Fennell, O. A. Petrenko, B. Fak, J. S. Gardner, S. T. Bramwell, B. Ouladdiaf, Phys. Rev. B 72, 224411 (2005)
41. K. Binder, A. P. Young, Rev. Mod. Phys. 58, 801 (1986)
42. S. T. Bramwell and M. J. Harris, J. Phys.: Condens. Matter 10, L215 ((1998)
43. In Refs. [30,31], a quantity $J_{nn} = J=3$ and $D_{nn} = 5D=3$ between the z_i Ising variables was employed. The reason for introducing these two rescaled couplings becomes clear when considering Eq. (1.14)
44. X. Ke, R. S. Freitas, B. G. Ueland, G. C. Lau, M. L. Dahlberg, R. J. Cava, R. Moessner, P. Schier, Phys. Rev. Lett. 99, 137203 (2007)
45. B. C. den Hertog, M. J. P. Gingras, S. T. Bramwell, M. J. Harris, arXiv:cond-mat/9912220 (1999)
46. A. L. Cornelius, J. S. Gardner, Phys. Rev. B, 64, 060406 (2001)
47. H. Kadowaki, Y. Ishii, K. Matsuhira, Y. Hinatsu, Phys. Rev. B 65, 144421 (2002)
48. X. Ke, B. G. Ueland, D. V. West, M. L. Dahlberg, R. J. Cava, P. Schier, Phys. Rev. B 76, 214413 (2007)
49. R. G. Melko, B. C. den Hertog, M. J. P. Gingras, Phys. Rev. Lett. 87, 067203 (2001)
50. R. G. Melko, M. J. P. Gingras, J. Phys.: Condensed Matter 16, R1277 (2004)
51. C. Kittel, Introduction to Solid State Physics, 8th edn. (Wiley, 2005), Appendix B
52. M. J. P. Gingras, B. C. den Hertog, Can. J. Phys. 79, 1339 (2001)
53. J. N. Reimers, A. J. Berlinsky, A. C. Shi, Phys. Rev. B 43, 865 (1991)
54. M. Enjalbal, M. J. P. Gingras, Phys. Rev. B 70, 174426 (2004)
55. S. V. Isakov, R. Moessner, S. L. Sondhi, Phys. Rev. Lett. 95, 217201 (2005)
56. M. Enjalbal, M. J. P. Gingras, arXiv:cond-mat/0307151v1 (2003)
57. H. Fukazawa, R. G. Melko, R. Higashinaka, Y. Maeno, M. J. P. Gingras, Phys. Rev. B 65, 054410 (2002)
58. G. T. Barkema, M. E. J. Newman, Phys. Rev. E 57, 1155 (1998)
59. M. E. J. Newman and G. T. Barkema, Monte Carlo Methods in Statistical Physics, (Clarendon Press, Oxford, 1999)
60. S. V. Isakov, K. Gregor, R. Moessner, S. L. Sondhi Phys. Rev. Lett. 93, 167204 (2004)
61. C. Castelnovo, R. Moessner, S. L. Sondhi, Nature 451, 42 (2008)
62. L. D. C. Jaubert, P. C. W. Holdsworth, arXiv:0903.1074 (2009). To appear in Nature Physics (2009).
63. R. Moessner, S. L. Sondhi, Phys. Rev. B 68, 064411 (2003)
64. Y. Tabata, H. Kadowaki, K. Matsuhira, Z. Hiroi, N. Aso, E. Ressouche, Fak, Phys. Rev. Lett. 97, 257205 (2006)
65. T. Fennell, S. T. Bramwell, D. F. McMorrow, P. Manuel, A. R. Wildes, Nature Physics 8, 566 (2007)
66. R. Higashinaka, Y. Maeno Phys. Rev. Lett. 95, 237208 (2005)
67. L. Jaubert, J. T. Chalker, P. C. W. Holdsworth, R. Moessner, Phys. Rev. Lett. 100, 067207 (2008)

68. Z. Hiroi, K. Matsuhira, M. Ogata, J. Phys. Soc. Jpn. 72, 3045 (2003)
69. S.-i. Yoshida, K. Nemoto, K. Koh Wada, J. Phys. Soc. Jpn. 73, 1619 (2004)
70. J. P. C lancy, J. P. C. Ru , S. R. D unsiger, Y. Zhao, H. A. D abkowska, J. S. G ardner, Y. Q iu, J. R. D. C opley, T. Jenkins, B. D. G aulin, Phys. Rev. B 79, 014408 (2009)
71. T. Sakakibara, T. Tayama, Z. Hiroi, K. Matsuhira, S. Takagi, Phys. Rev. Lett. 90, 207205 (2003)
72. H. Aoki, T. Sakakibara, K. Matsuhira, Z. Hiroi, J. Phys. Soc. Jpn. 73, 2851 (2004)
73. M. J. Harris, S. T. Bramwell, P. C. W. Holdsworth, J. D. Champion, Phys. Rev. Lett. 81, 4496 (1998)
74. J. Snyder, B. G. Ueland, J. S. Slusky, H. Karunadasa, R. J. Cava, A. M ize, P. Schier, Phys. Rev. Lett. 91, 107201 (2003)
75. J. Snyder, B. G. Ueland, J. S. Slusky, H. Karunadasa, R. J. Cava, P. Schier, Phys. Rev. B 69, 064414 (2004)
76. G. Ehlers, J. S. Gardner, C. H. Booth, M. Daniel, K. C. Kam, A. K. Cheetham, D. Antonio, H. E. Brooks, A. L. Cornelius, S. T. Bramwell, J. Lago, W. Haussler, N. Rosov Phys. Rev. B 73, 174429 (2006)
77. J. P. Sutter, S. T. Sutsui, R. Higashinaka, Y. Maeno, O. Leupold, A. Q. Baron, Phys. Rev. B 75, 140402 (2007)
78. J. Lago, J. S. J. Blundell, C. Baines, J. Phys.: Condensed Matter 19, 326210 (2007)
79. G. Ehlers, E. Mamontov, M. Zampori, K. C. Kam, J. S. Gardner, Phys. Rev. Lett. 102, 016405 (2009)
80. S. Nakatsuji, Y. Machida, Y. Maeno, T. Tayama, T. Sakakibara, J. van Duijn, L. Balicas, J. N. Millican, R. T. M. Aluso, J. Y. Chan, Phys. Rev. Lett. 96, 087204 (2006)
81. Y. Machida, S. Nakatsuji, Y. Maeno, T. Tayama, T. Sakakibara, S. Onoda, Phys. Rev. Lett. 98, 057203 (2007)
82. A. Ikeda, H. Kawamura, J. Phys. Soc. Jpn. 77, 073707 (2008)
83. R. F. Wang, C. Nisoli, R. S. Freitas, J. Li, W. M. Conville, B. J. Cooley, M. S. Lund, N. Samarth, C. Leighton, V. H. Crespi, P. Schier, Nature 439, 303 (2006)
84. C. Nisoli, R. F. Wang, J. Li, W. F. M. Conville, P. E. Lammert, P. Schier, V. H. Crespi, Phys. Rev. Lett. 98, 217203 (2007)
85. A. Libal, C. Reichhardt, C. J. Reichhardt Phys. Rev. Lett. 97, 228302 (2006)
86. G. C. Lau, R. S. Freitas, B. G. Ueland, B. D. Muegge, E. L. Duncan, P. Schier, R. J. Cava, Nature Physics 2, 249 (2006)
87. G. C. Lau, B. D. Muegge, T. M. M. Queen, E. L. Duncan, R. J. Cava, J. Sol. State Chemistry 179, 3136 (2006)
88. G. C. Lau, R. S. Freitas, B. G. Ueland, M. L. Dahlberg, Q. Huang, H. W. Zandbergen, P. Schier, R. J. Cava, Phys. Rev. B 76, 054430 (2007)
89. P. Dalm as de Reotier, A. Yaouanc, L. Keller, A. Cervellino, B. Roessli, C. Baines, A. Forget, C. Vaji, P. C. Gubbens, A. Amato, P. J. King Phys. Rev. Lett. 96, 127202 (2006)
90. F. Bert, P. Mendels, A. O larii, N. Blanchard, G. Collin, A. Amato, C. Baines, A. D. Hillier, Phys. Rev. Lett. 97, 117203 (2006)
91. S. R. G blin, J. D. Champion, H. D. Zhou, C. R. Wiebe, J. S. Gardner, I. Terry, S. Calder, T. Fennell, S. T. Bramwell, Phys. Rev. Lett. 101, 237201 (2008)

92. H. D. Zhou, C. R. Wiebe, J. A. Janik, L. Balicas, Y. J. Yo, Y. Qiu, J. R. Copley, J. S. Gardner, *Phys. Rev. Lett.* 101, 227204 (2008)